

# Self-organization of microcircuit structure in networks of spiking neurons with plastic synapses

Gabriel Koch Ocker<sup>1,3\*</sup>, Ashok Litwin-Kumar<sup>2,3</sup>, Brent Doiron<sup>2,3</sup>

**1** Department of Neuroscience, University of Pittsburgh, Pittsburgh, PA, United States of America

**2** Department of Mathematics, University of Pittsburgh, Pittsburgh, PA, United States of America

**3** Center for the Neural Basis of Cognition, University of Pittsburgh and Carnegie Mellon University, Pittsburgh, PA, United States of America

\* E-mail: gko1@pitt.edu

## Abstract

The microcircuit structure of cortical networks features an abundance of certain wiring motifs, especially compared to simple random-network models. This structure is not hardwired, but rather emerges from activity-dependent plasticity rules that govern the synaptic connections between cells. A majority of theoretical studies of plastic networks consider the effect of external training on shaping network architecture. We study the complementary situation of how a recurrent network with plastic synapses interacts with spontaneous spiking dynamics to create self-organized network structure. We develop a self-consistent theory that combines fast spike-time correlations, computed using a linear response framework, with an fast-slow theory for synaptic weight dynamics to describe the evolution of network architecture. With a finite-size expansion of network dynamics we obtain a low-dimensional set of nonlinear differential equations for the evolution of two-synapse motif structure within the network. With this theory in hand, we give a principled exploration of how the details of the plasticity rule drive the evolution of microcircuit structure in cortical networks.

## Author Summary

The connectivity of mammalian brains exhibits structure at a wide variety of spatial scales, from the broad (which brain areas connect to which) to the extremely fine (where synapses from different inputs lie on the morphology of individual neurons). Recent experimental work in the neocortex has highlighted structure at the level of microcircuits: different patterns of connectivity between small groups of neurons are either more or less abundant than would be expected by chance. A central question in circuit neuroscience is how this structure emerges. Attempts at an answer are confounded by the known mutual interaction of network architecture and spiking activity. Indeed, the wiring of synaptic connections influences spiking statistics, while individual synapses are highly plastic and become stronger or weaker depending on the activity of the pre- and post-synaptic neurons. We present a self-consistent theory for how activity-dependent synaptic plasticity shapes the microcircuit structure of neuronal networks, and use it to show how the shape of the plasticity rule can govern the promotion or suppression of different connectivity patterns. Our work provides a foundation for understanding how cortical circuits, and not just individual synapses, are malleable in response to inputs both external and internal to a network.

## Introduction

The wiring of neuronal networks exhibits structure across a broad range of spatial scales [1]. In particular, patterns of connectivity among small groups of excitatory neurons are over- or under-represented compared to random networks [2–5]. The prevalence of these motifs is related to a neuron’s stimulus preferences and activity levels, and is correlated with the temporally patterned spiking activity in neural circuits [6, 7].

Motivated in part by these observations, there is a growing body of theoretical work that discusses how wiring structure dictates the spiking activity of cortical neurons [8–14].

While neural architecture undoubtedly plays a strong role in determining neuronal activity, the reverse is also true. Individual synapses can both potentiate (strengthen) and depress (weaken), and whether they do so depends on the relative timing of action potentials in the connected neurons [15, 16]. Such *spike timing-dependent plasticity* (STDP) has featured prominently in both experimental and theoretical studies of neural circuits [17–19]. Of particular interest, STDP provides a mechanism for Hebbian plasticity of neural circuits; synapses where the presynaptic neuron reliably drives the postsynaptic one tend to potentiate while in the reverse case, synapses depress [20]. Hebbian plasticity is a central mechanism that links circuit structure and functional neural dynamics. This is accomplished by forming heavily wired assemblies of neurons, where assembly membership is associated with coordinated, elevated firing rates during a specific computation [21]. This idea, originally proposed by Hebb [22], has gained significant evidence in both hippocampus [23] and sensory cortex [24].

Despite the promise of STDP providing insight into the wiring of large-scale neural circuits, many studies of STDP have focused on the plasticity of synaptic connections between just a single pair of pre- and post-synaptic neurons [20, 25–28]. In those studies, when depression is slightly stronger compared to potentiation or postsynaptic spikes drive depression in addition to STDP, then a neuron’s firing rate can stabilize. If some inputs are temporally correlated then they will more reliably drive postsynaptic spikes and cooperate to all potentiate, while uncorrelated inputs may depress [20, 29–31]. This rule then generates a feedforward circuit [32], a scenario that is divorced from activity in the neocortex, where spiking activity is shaped by the structure of recurrent networks. A central challenge for theories of synaptic plasticity in recurrent networks is to elucidate the two-way interaction between network structure and spiking activity.

Due to this challenge, many studies have resorted to large scale numerical simulations of cortical networks with plastic synapses [33–36]. While intuition for the development of circuit structure can be gained using this approach, without a governing theoretical framework it is often difficult to extract generalized principles. Alternatively, mathematical analyses have been restricted to either small networks [35, 37], or required Poisson neurons [38–41]. The latter works considered the only source of correlations to be shared inputs from outside the network, and did not consider correlated spiking activity due to internal coupling within the network. Thus, there is a need for a simple mathematical framework that captures how STDP drives self-organization of circuit structure in recurrently coupled cortical networks.

To this end, we construct a self-consistent theory for the coevolution of spiking statistics and synaptic strengths in networks with STDP. This theory makes use of a previously developed linear response framework for calculating joint spiking statistics [13, 42, 43] and a separation of timescales between spiking correlations and synaptic plasticity [29]. Most previous studies of plasticity in recurrent networks have focused on how they can be trained to represent an external stimulus. We focus on how spiking covariability generated by interactions within the network interacts with plasticity to shape network structure. We then use this high-dimensional theory to derive a low-dimensional, closed system for the STDP of motifs in recurrent networks. This reveals instabilities in the motif dynamics, which impose thresholds for the promotion or suppression of different motifs. This theory for motif plasticity also highlights the circumstances in which spike-time covariations, in contrast to firing rates, control the STDP of motifs.

## Results

### Spike train correlations drive synaptic plasticity

We begin by reviewing a well studied phenomenological model of spike timing-dependent plasticity (STDP) [44], acting within a simple two neuron reciprocally coupled circuit. Consider a pair of pre- and post-synaptic spike times with time lag  $s = t_{\text{post}} - t_{\text{pre}}$ . The evolution of the synaptic weight connecting cell  $j$  to cell  $i$  obeys  $\mathbf{W}_{ij} \rightarrow \mathbf{W}_{ij} + L(s)$ , with the STDP rule  $L(s)$  (Fig. 1A) being Hebbian:

$$L(s) = \begin{cases} \mathcal{H}(W^{\text{max}} - \mathbf{W}_{ij}) f_+ e^{-\frac{|s|}{\tau_+}}, & \text{if } s \geq 0 \\ \mathcal{H}(\mathbf{W}_{ij}) (-f_-) e^{-\frac{|s|}{\tau_-}}, & \text{if } s \leq 0, \end{cases} \quad (1)$$

Here  $\mathcal{H}(x) = 1$  if  $x > 0$  while  $\mathcal{H}(x) = 0$  if  $x < 0$ , imposing bounds on the weights to prevent excitatory synapses from depressing into being inhibitory or from potentiating unlimitedly (i.e.  $0 \leq \mathbf{W}_{ij} \leq W^{\text{max}}$ ). The coefficients  $f_{\pm}$  scale the amplitude of weight changes induced by individual pre-post spike pairs and  $\tau_{\pm}$  determine how synchronous pre- and post-synaptic spikes must be to drive plasticity.

The spike train from neuron  $i$  is the point process  $\mathbf{y}_i(t) = \sum_k \delta(t - t_{ik})$ , with  $t_{ik}$  being the  $k^{\text{th}}$  spike-time from neuron  $i$ . Following [29] we relate the joint statistics of  $\mathbf{y}_i(t)$  and  $\mathbf{y}_j(t)$  to the evolution of synaptic weights. We first assume that individual pre-post spike pairs induce small changes in synaptic weights ( $f_{\pm} \ll W^{\text{max}}$ ). This makes the synaptic weights evolve slowly, on a much longer timescale than the millisecond scale of pairwise spike-time covariability due to network interactions. The separation of timescales between synaptic plasticity and spiking activity provides an approximation to the evolution of the synaptic weights (Methods: learning dynamics):

$$\frac{d\mathbf{W}_{ij}}{dt} = \mathbf{W}_{ij}^0 \int_{-\infty}^{\infty} L(s) (r_i r_j + \mathbf{C}_{ij}(s)) ds. \quad (2)$$

Here  $r_i = \langle \mathbf{y}_i(t) \rangle$  is the time-averaged firing rate of neuron  $i$ , and  $\mathbf{C}_{ij}(s) = \langle (\mathbf{y}_i(t) - r_i)(\mathbf{y}_j(t+s) - r_j) \rangle$  is the cross-covariance function of neuron  $i$  and  $j$ 's spike trains. The term  $r_i r_j$  in Eq. (2) captures the firing rate dependence of STDP, while  $\mathbf{C}_{ij}(s)$  models the sensitivity of STDP to spike timing. Finally,  $\mathbf{W}^0$  is the adjacency matrix of the network – a binary matrix with  $\mathbf{W}_{ij}^0 = 1$  denoting the presence of a synapse. Multiplying by  $\mathbf{W}_{ij}^0$  ensures that synapses that do not exist cannot potentiate into existence. Eq. (2) requires only the first and second order joint spiking statistics. To facilitate calculations many previous studies have used Poisson neuron models with a specified  $r_i$  and  $\mathbf{C}_{ij}(s)$  as a simple generator for  $\mathbf{y}_i(t)$ . In contrast, we will use a white noise driven exponential integrate-and-fire model [45] for the generation of spike times (Methods: Network model). While this complicates the calculation of the spike-train statistics, it provides a biophysically realistic model of neural dynamics [46, 47] that better captures the timescales and cellular nonlinearities that shape  $r_i$  and  $\mathbf{C}_{ij}(s)$ .

In total, the above theory determines synaptic evolution from the integrated combination of an STDP rule  $L(s)$  and the spike-train correlation  $\mathbf{C}_{ij}(s)$ . Thus, any mechanism affecting two neurons' spiking covariability is expected to shape network structure through STDP. As a simple illustration of this we examined the synaptic weight dynamics,  $\mathbf{W}_{12}(t)$  and  $\mathbf{W}_{21}(t)$ , in a reciprocally coupled pair of neurons, both in the presence and absence of common inputs. Specifically, the fluctuating input to neuron  $i$  was the sum of a private and common term,  $\sqrt{1-c}\xi_i(t) + \sqrt{c}\xi_c(t)$ , with  $c$  being the degree of correlation between the inputs to the cells. In the absence of common input ( $c = 0$ ; Fig. 1B), the two synapses behaved as expected with Hebbian STDP; one synapse potentiated and the other depressed (Fig. 1C). By comparison, the presence of common input ( $c = 0.05$ ) was a source of synchrony in the two neurons spike trains, inducing a central peak in the spike train cross-covariance function  $\mathbf{C}_{ij}(s)$  (Fig. 1B vs 1D). In

this case both synapses potentiated (Fig 1E). This was because the common input increased synchronous spiking, thereby enhancing the degree of overlap between  $\mathbf{C}_{ij}(s)$  and the potentiation component of  $L(s)$ . This overcame the depression dynamics in the initially weaker synapse, and promoted strong, bidirectional connectivity in the two cell circuit.

This example highlights how the temporal shaping of spiking covariability can direct spike timing-dependent plasticity. However, this case only considered the effect of correlated inputs from outside of the modeled circuit (Fig 1). Our primary goal is to predict how intrinsically generated spike-time covariability due to internal network interactions combines with STDP to dynamically drive self-organized network architecture. In order to do this, we first require a theory for predicting the full structure of spike-train covariances from a static, recurrent network connectivity.

### Network architecture determines spike train correlations in static networks

In this section we review approximation methods [13, 42] that estimate pairwise spike train correlation  $\mathbf{C}_{ij}(s)$  using a static weight matrix  $\mathbf{W}$ . The exposition is simplified if we consider the Fourier transform of a spike train,  $\mathbf{y}_i(\omega) = \int_{-\infty}^{\infty} \mathbf{y}_i(t) e^{-2\pi i \omega t} dt$ , where  $\omega$  is frequency in radians. Assuming weak synaptic connections  $\mathbf{W}_{ij}$ , we approximate the spike response from neuron  $i$  as:

$$\mathbf{y}_i(\omega) = \mathbf{y}_i^0(\omega) + \mathbf{A}_i(\omega) \left( \sum_{j=1}^N \mathbf{W}_{ij} J(\omega) \mathbf{y}_j(\omega) \right). \quad (3)$$

The function  $\mathbf{A}_i(\omega)$  is the linear response of the postsynaptic cell, measuring how strongly modulations in synaptic currents at frequency  $\omega$  are transferred into modulations of instantaneous firing rate about a background state  $\mathbf{y}_i^0$ . The function  $J(\omega)$  is a synaptic filter. In brief, Eq. (3) is a linear ansatz for how a neuron integrates and transforms a realization of synaptic input into a spike-train realization.

Following [13, 42] we use this linear approximation to estimate the Fourier transform of  $\mathbf{C}_{ij}(t)$ , written as  $\mathbf{C}_{ij}(\omega) = \langle \mathbf{y}_i(\omega) \mathbf{y}_j^*(\omega) \rangle$ ; here  $\mathbf{y}^*$  denotes complex conjugation. This yields the following matrix equation:

$$\mathbf{C}(\omega) = \left( \mathbf{I} - (\mathbf{W} \cdot \mathbf{K}(\omega)) \right)^{-1} \mathbf{C}^0(\omega) \left( \mathbf{I} - (\mathbf{W} \cdot \mathbf{K}^*(\omega)) \right)^{-1}, \quad (4)$$

where  $\mathbf{K}(\omega)$  is an interaction matrix defined by  $\mathbf{K}_{ij}(\omega) = \mathbf{A}_i(\omega) \mathbf{J}_{ij}(\omega)$ . The expression  $\mathbf{C}^0(\omega)$  is the baseline covariance matrix, with element  $\mathbf{C}_{ij}^0(\omega) = \langle \mathbf{y}_i^0(\omega) \mathbf{y}_j^{0*}(\omega) \rangle$ , and  $\mathbf{I}$  is the identity matrix. Using Eq. (4) we recover the matrix of spike train cross-covariance functions  $\mathbf{C}(t)$  by inverse Fourier transformation. Thus, Eq. (4) provides an estimate of the statistics of pairwise spiking activity in the full network, taking into account the full network structure (see Methods: Spiking statistics for a full description of Eqs. (3) and (4)).

As a demonstration of the theory we examined the spike-train covariances of three neurons from a 1000-neuron network (Fig 2A, colored cells). The synaptic weight matrix  $\mathbf{W}$  was static and had an adjacency matrix  $\mathbf{W}^0$  that was randomly generated with Erdős-Rényi statistics (connection probability of 0.15). The neurons received no correlated input from outside the network, making  $\mathbf{C}^0(\omega)$  a diagonal matrix, and thus recurrent network interactions were the only source of spike train covariability. Nevertheless, the structure of network connections dictates the shape of spike-train covariances. Neuron pairs that connect reciprocally with equal synaptic weights have temporally symmetric spike-train covariances (Fig 2C), while uni-directional connections give rise to temporally asymmetric spike-train covariances (Fig 2D). When neurons are not directly connected, their spiking covariability is weaker than that of directly connected neurons but is still nonzero (Fig 2E). The theoretical estimate provided by Eq. (4) was in good agreement with estimates from direct simulations of the network (Fig. 2C,D,E red vs. gray curves).

## Self-consistent theory for network structure and spiking correlations with plastic synapses

In general, it is challenging to develop theoretical techniques for stochastic systems with several variables and nonlinear coupling [48], such as in Eq. (2). Fortunately, in our model the timescale of spiking correlations in the recurrent network with static synapses is on the order of milliseconds (Fig. 2C,D,E), while the timescale of plasticity is minutes (Fig. 1C,E). This separation of timescales provides an opportunity for a self-consistent theory for the coevolution of  $\mathbf{C}(s)$  and  $\mathbf{W}(t)$ . More to the point, so long as  $f_{\pm}$  in Eq. (1) are sufficiently small, then we can approximate  $\mathbf{W}$  as static over the timescales of  $\mathbf{C}(s)$  and insert Eq. (4) into Eq. (2). The resulting system yields a solution  $\mathbf{W}(t)$  that captures the long timescale dynamics of the plastic network structure (Methods: self-consistent theory for network plasticity).

As a first illustration of our theory we focus on the evolution of three synaptic weights in a 1000-neuron network (Fig. 3A, colored arrows). The combination of Eqs. (2) and (4) predicted the dynamics of  $\mathbf{W}(t)$ , whether the weight increased with time (Fig. 3B left, red curve), decreased with time (Fig. 3C left, red curve), or remained approximately constant (Fig. 3D left, red curve). In all three cases the theory matched well the average evolution of the synaptic weight estimated from direct simulations of the spiking network (Fig. 3B,C,D left, thick black curves). Snapshots of the network at three time points (axis arrows in Fig. 3B,C,D, left), showed that  $\mathbf{W}$  coevolved with the spike train covariance (Fig. 3B,C,D right). We remark that for any realization of background input  $\mathbf{y}^0(t)$ , the synaptic weights  $\mathbf{W}(t)$  deviated from the average value with increasing spread (Fig. 3B,C,D left, thin black curves). This is expected since  $\mathbf{C}(t)$  is an average over realizations of  $\mathbf{y}^0(t)$ , and thus provides only a prediction for the drift of  $\mathbf{W}(t)$ , while the slow integration of  $\mathbf{W}(t)$  through Eq. (2) gives a significant diffusive character to  $\mathbf{W}(t)$  [29].

In sum, the fast-slow decomposition of spike train correlations and synaptic plasticity provides a coherent theoretical framework to investigate the formation of network structure through STDP. Also, our treatment is complementary to past studies on STDP [?, 31, 40, 49] that focused on the development of architecture through an external training signal. In our model, there are no correlations in the background states (i.e.  $\mathbf{C}_{ij}^0(s) = \langle \mathbf{y}_i^0(t+s)\mathbf{y}_j^0(t) \rangle = 0$  for  $i \neq j$ ), so we consider the self-organization of network structure through internally generated spike train correlations.

While our theory gives an accurate description of network plasticity, it is nevertheless high-dimensional. Keeping track of every individual synaptic weight and spike-train cross-covariance function involves  $\mathcal{O}(N^2)$  terms. For large networks, this becomes computationally intensive. More importantly, this high-dimensional theory does not provide insights into the plasticity of *connectivity patterns* or *motifs*, which are a hallmark of cortical networks [3, 4]. Motifs amongst two or more neurons represent correlations in the network's weight matrix, which cannot be described by a straightforward application of mean-field theoretic techniques. In the next section we develop a principled approximation of the high-dimensional theory to a closed low-dimensional mean-field theory for how the mean weight and the strength of two-synapse motifs evolves due to STDP.

## Motif plasticity

We begin by defining the two-synapse connectivity motifs:

$$\begin{aligned}
 p &= \frac{1}{N^2} \sum_{i,j} \mathbf{W}_{ij}, \\
 q^{\text{div}} &= \frac{1}{N^3} \sum_{i,j,k} \mathbf{W}_{ik} \mathbf{W}_{jk} - p^2, \\
 q^{\text{con}} &= \frac{1}{N^3} \sum_{i,j,k} \mathbf{W}_{ik} \mathbf{W}_{ij} - p^2, \\
 q^{\text{ch}} &= \frac{1}{N^3} \sum_{i,j,k} \mathbf{W}_{ij} \mathbf{W}_{jk} - p^2.
 \end{aligned} \tag{5}$$

The mean connection strength is  $p$ , while  $q^{\text{div}}$ ,  $q^{\text{con}}$  and  $q^{\text{ch}}$  respectively measure the strength of divergent, convergent, and chain motifs in the network. In each case, we subtract the motif strength in a network with independent weights,  $p^2$ , so that the  $q$ s measure above- or below-chance levels of structure in the network. Note that these motif variables depend on the strength of both synapses making up the motif.

In order to calculate the dynamic plasticity of, for example,  $p$ , we insert the slow-fast STDP theory of Eq. (2) into the first equation of (5):

$$\frac{dp}{dt} = \frac{1}{N^2} \sum_{i,j} \mathbf{W}_{ij}^0 \int_{-\infty}^{\infty} L(s) (r_i r_j + \mathbf{C}_{ij}(s)) ds \tag{6}$$

where the spike train covariances are calculated using linear response theory (Eq. (4)). This equation depends on the full network structure in two ways. First, it depends on the full adjacency matrix  $\mathbf{W}^0$ . Second, the spike train covariances depend on the full weight matrix:  $\mathbf{C}_{ij}(s) = \mathbf{C}_{ij}(s; \mathbf{W})$ . In a similar fashion, the dynamics of motifs  $q^{\text{div}}(t)$ ,  $q^{\text{con}}(t)$ , and  $q^{\text{ch}}(t)$  likewise depend on the full network structure. This dependence of first- and second-order connectivity statistics on the full network structure poses a challenge for the development of a closed theory for motif plasticity.

The main steps in our approach are three approximations. First, the covariance matrix  $\mathbf{C}(s)$  obtained from our linear ansatz (Eq. (4)) can be expanded in a power series around the background covariances  $\mathbf{C}^0$  (see Eq. (22)). Powers of the interaction matrix  $\mathbf{K}$  in this series correspond to path lengths through the network [12, 13]. We truncate the spike train covariances at length one paths through the network to obtain (Eq. (7)):

$$\mathbf{C}_{ij}(s) \approx \underbrace{(\mathbf{W}_{ij} \mathbf{K}_{ij} * \mathbf{C}_{jj}^0)}_{\text{forward connection}}(s) + \underbrace{(\mathbf{C}_{ii}^0 * \mathbf{W}_{ji} \mathbf{K}_{ji}^-)}_{\text{backward connection}}(s) + \underbrace{\sum_k (\mathbf{W}_{ik} \mathbf{K}_{ik} * \mathbf{C}_{kk}^0 * \mathbf{W}_{jk} \mathbf{K}_{jk}^-)}_{\text{common inputs}}(s), \tag{7}$$

where the symbol  $*$  denotes convolution. This truncation separates the various network sources of spike-train covariability between the spiking of neurons  $i$  and  $j$  into direct forward ( $i \leftarrow j$ ), backward ( $i \rightarrow j$ ), and common ( $k \rightarrow i$  and  $k \rightarrow j$ ) connections. Neglecting contributions to  $\mathbf{C}(s)$  from higher order connection motifs stops the two-synapse motifs from depending, through the spike-train correlations, on the full network structure.

Nevertheless, after truncating  $\mathbf{C}(s)$ , the first- ( $p$ ) and second-order ( $q^{\text{div}}$ ,  $q^{\text{con}}$ ,  $q^{\text{ch}}$ ) motifs still depend on higher order motifs. This is because of coupling between lower and higher-order moments of the connectivity matrix  $\mathbf{W}$  (see Eqs. (27)-(29)), and presents a significant complication. In order to close the motif dynamics at first- and second-order, our second approximation follows [14] and we rewrite higher-order motifs as combinations of individual synapses and two-synapse motifs (see Eqs. (34)-(35)). This corresponds to assuming that there are no third- or higher-order correlations in the weight matrix beyond those due to second-order correlations. The final approximation is to ignore the bounds on the synaptic weight in Eq. (1). While this forces a theory that only captures the transient dynamics of  $\mathbf{W}(t)$ , it greatly simplifies the derivation of a low dimensional theory of motif structure because dynamics along the boundary surface are not considered.

These approximations allow us (see Eqs. (24), (27), and (36)) to rewrite the dynamics of the mean connection strength  $p$  as:

$$\frac{dp}{dt} = p_0 r^2 S + \epsilon \left[ p S_F + (q_X^{\text{rec}} + p_0 p) S_B + \frac{1}{p_0} \left( p_0 (q^{\text{div}} + p^2) + p (q_X^{\text{con}} + q_X^{\text{ch,B}}) \right) S_C \right]. \quad (8)$$

The mean firing rate is  $r$  and  $p_0 = \frac{1}{N^2} \sum_{i,j} \mathbf{W}_{ij}^0$  is the connection density of the network. Since our theory for spiking covariances required weak synapses, we also explicitly scaled the weights and motifs, and the amplitude of synaptic changes  $f_{\pm}$  in Eq. (1), by  $\epsilon = 1/(Np_0)$ . This ensured that as connection probability  $p_0$  was varied, synaptic weights scaled to keep the total input to a neuron constant (neglecting plasticity).

The first term on the right hand side of Eq. (8) is scaled by  $S = \int_{-\infty}^{\infty} L(s) ds$ , modeling the interaction between the STDP net potentiation ( $S > 0$ ) or depression ( $S < 0$ ), and the mean firing rate across the network. The remaining terms capture how synaptic weights interact with the temporal covariability of spiking in the network. Because of the expansion in Eq. (7) these dependencies decompose into three terms, each scaled by the integral of the STDP rule  $L(s)$  and a component of the spike train correlation  $\mathbf{C}(s)$ . Specifically, correlations due to forward connections are represented by  $S_F$  (Eq. (31); Fig. 4A), correlations due to backward connections are represented by  $S_B$  (Eq. (32); Fig. 4B), and finally correlations due to common connections are represented by  $S_C$  (Eq. (33); Fig. 4C). The dynamics of  $p(t)$  will involve the interactions of different motifs through all of these components.

In Eq. (8), the impact of forward correlations through  $S_F$  is proportional to the mean connection strength  $p$ . In contrast, the backward correlations  $S_B$  must interact with the new variable  $q_X^{\text{rec}}$ , which measures the mean strength of connections conditioned on their being part of a reciprocal loop (i.e the backward connection must exist). In a similar fashion, the correlations from common input  $S_C$  involve  $p$ , divergent connections,  $q^{\text{div}}$ , as well as terms conditioned on weights being part of a convergent motif,  $q_X^{\text{con}}$ , or on the postsynaptic neuron making another synapse in a chain,  $q_X^{\text{ch,B}}$ . The definitions for the mixed motifs, the  $q_X$ s, are given in Eqs. (21). In total, the dynamics of mean synaptic strength cannot be written as a single closed equation, but also requires knowledge of how the second order motifs evolve.

Fortunately, using a similar approach, dynamical equations can be derived for each of the two-synapse motifs  $q^{\text{div}}$ ,  $q^{\text{cov}}$ , and  $q^{\text{ch}}$  (Eqs. (37)-(39)). However, to close the system we require dynamics for five mixed motifs,  $q_X^{\text{con}}$ ,  $q_X^{\text{div}}$ ,  $q_X^{\text{rec}}$ ,  $q_X^{\text{ch,A}}$ , and  $q_X^{\text{ch,B}}$  (Eqs. (40)-(44)). The inclusion of mixed motifs stems from the presence of the adjacency matrix  $\mathbf{W}^0$  in Eq. (2). They correspond to the mean strength of individual connections, conditioned on their being part of a particular motif. In total, this yields an autonomous 4 + 5 dimensional system of nonlinear differential equations describing the population averaged plasticity of second-order network structure. We have derived these equations in the absence of common external inputs to the neurons; the theory can easily be extended to this case by including external correlations in Eq. (7) (replacing  $\mathbf{C}^0$  with  $(\mathbf{C}^0 + \mathbf{C}^{\text{ext}})$ , where  $\mathbf{C}^{\text{ext}}$  is the covariance matrix of the inputs).

The mean field theory of Eqs. (36)-(44) gives an accurate prediction of the transient dynamics of the first- and second-order motif structure of the full stochastic spiking network with plastic synapses (Fig. 5, compare red versus thin black curves), owing to significant drift compared to diffusion in the weight dynamics and these network-averaged motif strengths. The derivation and successful application of the reduced theory to the problem of self-organization of network structure in spiking networks with plastic synapses is a central result of our study.

Our second-order motif theory captures several nontrivial aspects of the evolution of network structure. First, while the STDP rule is in the depression-dominated regime ( $S < 0$  for the simulations in Fig. 5), the mean connection strength  $p$  nevertheless grows (Fig. 5A). Second, both divergent and convergent connections,  $q^{\text{div}}$  and  $q^{\text{con}}$ , grow above what is expected for a random (Erdős-Rényi) graph (Fig. 5B,C); however, at the expense of chain connections  $q^{\text{ch}}$  which reduce in magnitude (Fig. 5G). In the subsequent sections we leverage the simplicity of our reduced theory to gain insight into how the STDP rule  $L(s)$  interacts with recurrent architecture to drive self-organized motif dynamics in plastic networks.

## Unbalanced STDP

The motif dynamics each contain one term proportional to the firing rates and integral of the STDP rule,  $r^2 S$ , and additional terms proportional to the small parameter  $\epsilon$ . When  $L(s)$  is strongly dominated by either depression or potentiation (so that  $S \sim \mathcal{O}(1) \gg \epsilon$ ) the whole network uniformly depresses (Fig. 6A) or potentiates (Fig. 6B) due to chance spike coincidences (the firing rate term dominates in Eq. (2)). These dynamics are straightforward at the level of individual synapses, but what do they correspond to for the motifs?

When the STDP rule is strongly dominated by potentiation or depression, the  $\mathcal{O}(\epsilon)$  terms in Eqs. (37)-(44) are negligible; each motif's plasticity is solely determined by the firing rates, with spike-time covariability playing no role. In this simple case, the motif dynamics are:

$$\begin{aligned}\frac{dp}{dt} &= p_0 r^2 S + \mathcal{O}(\epsilon) \\ \frac{dq^\alpha}{dt} &= 2r^2 S q_X^\alpha + \mathcal{O}(\epsilon) \\ \frac{dq_X^\alpha}{dt} &= r^2 S q_0^\alpha + \mathcal{O}(\epsilon)\end{aligned}\tag{9}$$

for  $\alpha = \text{div}, \text{con}, \text{or ch}$  (and taking  $q_X^{\text{ch}} = (q_X^{\text{ch,A}} + q_X^{\text{ch,B}})/2$  in the second equation). Dropping order  $\epsilon$  terms gives the simple solutions:

$$\begin{aligned}p(t) &= p_0 r^2 S t + p(0) \\ q^\alpha(t) &= q^\alpha(0) + q_X^\alpha(0) r^2 S t + \frac{1}{2} q_0^\alpha (r^2 S)^2 t^2\end{aligned}\tag{10}$$

for  $\alpha = \text{div}, \text{con}, \text{or ch}$  (Methods: Unbalanced STDP). This gives linear decay or growth (for depression- or potentiation-dominated  $L(s)$ , respectively) of  $p$  with  $r^2$ , and the two-synapse motif strengths quadratically amplify the frequencies of these motifs in the baseline network structure  $\mathbf{W}^0$ . In other words, the uniform plasticity of individual weights eventually amplify the motif structure that is initially present, whether that is to over-represent ( $q_0 > 0$ ) or under-represent ( $q_0 < 0$ ) the motif frequency.



## Balanced STDP of the mean synaptic weight

When there is a balance between potentiation and depression, so that  $S \sim \mathcal{O}(\epsilon)$ , then all terms of the motif dynamics, in principle, contribute to the evolution of Eqs. (37)-(44). We begin the analysis of the balanced STDP case by noting the existence of an invariant set for independently weighted networks. When the network structure,  $\mathbf{W}^0$  is approximately Erdős-Rényi the motif frequencies  $q_0$  are  $\mathcal{O}(N^{-3/2}) = \mathcal{O}(\epsilon^{3/2})$ . If we further assume initial conditions for the motif strengths and the mixed motifs to be consistent with Erdős-Rényi statistics ( $q(0) = \mathcal{O}(\epsilon^{3/2})$  for all motifs), then we also have  $dq_X/dt = \mathcal{O}(\epsilon^{3/2})$  and  $dq_X/dt = \mathcal{O}(\epsilon^{3/2})$  for all the motif dynamics, Eqs. (37)-(44).

In this case we can neglect, to leading order, the motif dynamics entirely. So, for independently weighted networks the dynamics evolve on the invariant set  $\{p(t), q^{\text{div}} = q^{\text{con}} = q^{\text{ch}} = q_X^{\text{rec}} = q_X^{\text{con}} = q_X^{\text{div}} = q_X^{\text{ch,A}} = q_X^{\text{ch,B}} = 0\}$ . We start by examining this one-dimensional system for  $p$ .

In order to make explicit the balance between potentiation and depression, we write  $S = \pm\delta\epsilon$  (with  $+\delta$  for STDP with the balance tilted in favor of potentiation, and  $-\delta$  for balance tilted in favor of depression). On the invariant set, the leading-order dynamics of  $p$  are:

$$\frac{1}{\epsilon} \frac{dp}{dt} = \pm\delta p_0 r^2 + p(S_F + p_0 S_B) + p^2 S_C. \quad (11)$$

This quadratic equation admits two fixed points, one stable and the other unstable. The first question is whether either of these fixed points can be attained; do they lie inside the bounds  $[0, p_0 W^{\text{max}}]$ ? We begin by examining this for perfectly balanced potentiation and depression ( $\delta = 0$ ). The fixed points of  $p$  are then at 0 and  $-(S_F + p_0 S_B)/S_C$ . So the balance between  $S_F$  and  $p_0 S_B$  and the sign of  $S_C$  determine whether the second fixed point will be below or above zero, and whether it is attracting or repelling. This depends on the shapes of the STDP rule and the spike-train covariances.

Experimentally measured STDP rules in cortex often show  $f_+ > f_-$  and  $\tau_+ < \tau_-$  [50, 51], making potentiation windows ( $L(s)$  for  $s > 0$ ) sharper and higher-amplitude than depression windows ( $L(s)$  for  $s < 0$ ). In this case, the STDP-weighted correlations from forward connections,  $S_F > 0$ , are greater in magnitude than those from backward connections,  $S_B < 0$  (Fig. 4). Since  $0 < p_0 \leq 1$  then we have that  $S_F + p_0 S_B > 0$  and the sign of  $S_C$  determines whether the second fixed point is positive or negative. Since the correlations from common input decay symmetrically around  $s = 0$ , we have that  $S_C > 0$ , and the second fixed point will be below the bounds. Additionally, that second fixed point is stable and the fixed point at 0 is unstable, so that  $p$  will increase towards  $p_0 W^{\text{max}}$ .

When  $\delta \neq 0$ , the stable fixed point still lies below the unstable one and outside of the bounds  $[0, p_0 W^{\text{max}}]$ . So, it cannot be accessed and the location of the unstable fixed point determines whether  $p$  will potentiate or depress. For potentiation-dominated balanced STDP,  $+\delta$  in Eq. (11), both fixed points are negative and the value of the unstable fixed point decreases with the connection density  $p_0$ . In this case, the only depressing term is  $pp_0 S_B$  in Eq. (11), and it cannot compete with the remaining potentiating terms  $\delta p_0 r^2 S + S_F$ . Thus, the unstable fixed point pushes  $p$  away from itself, so the mean connection strength always potentiates with potentiation-dominated balanced STDP (Fig. 7A). Thus, while the timescale for potentiation is slower for potentiation-dominated balanced STDP, compared to that for unbalanced potentiation, the end result of net potentiation for all initial conditions  $p(0)$  and connection densities  $p_0$  is similar. That is not the case, however, when the balance is tilted towards depression.

With depression-dominated balanced STDP ( $-\delta$  in Eq. (11)) the fixed points are:

$$p^* = \frac{-(S_F + p_0 S_B) \pm \sqrt{(S_F + p_0 S_B)^2 + 4\delta p_0 r^2 S_C}}{2S_C}. \quad (12)$$

If  $f_+ > f_-$  and  $\tau_+ < \tau_-$ , then  $S_F > S_B$  so the term  $(S_F + p_0 S_B) > 0$ . Since  $S_C > 0$  in this case also, the term inside the square root is positive and one fixed point is positive and the other negative. The positive fixed point is unstable and, if within  $[0, p_0 W^{\max}]$ , provides a separatrix between potentiation and depression (Fig. 7B). This bistability arises from the competition between potentiation (due to forward correlations and common input) and depression (due to backward connections and firing rates).

We then investigated how the density of connections affected the plasticity of the mean connection strength. Examination of Eq. (12) shows competing effects of increasing  $p_0$ : it moves both fixed points closer to 0 (the  $p_0 S_B$  terms outside and inside the square root), but also pushes the fixed points away from 0 due to firing rate- and common-input-driven STDP. The latter effect dominates for the positive fixed point (Fig 7B). In total, we see that a slight propensity for depression can impose bistability on the mean synaptic weight.

## Balanced STDP of two-synapse motifs

Now, we turn our attention to how intrinsically generated spiking covariability interacts with balanced STDP to shape motif structure, examining the dynamics of Eqs. (36)-(44) off of the Erdős-Rényi invariant set. When the second-order motifs are not neglected, there is an unstable manifold in the 9-dimensional motif space, analogous to the unstable fixed point on the invariant set. Since it is off of the origin, this unstable manifold provides a threshold for the promotion or suppression of different motifs. We illustrate this by examining a slice through motif space: the  $(q^{\text{div}}, q^{\text{con}})$  plane. For STDP rules with a balance tilted towards depression ( $\delta < 0$ ), the unstable manifold provides a threshold for the promotion or suppression of connectivity patterns (Fig. 8A). The flow in this slice of the motif space predicts the dynamics of convergent and divergent motifs well (Fig. 8A, compare individual realizations of the full spiking network - thin black lines - to the flow defined by the vector field of the reduced motif system). This was the case even though the vector field is calculated by assuming that all other 7 variables in the system are held fixed at their initial conditions.

For STDP rules with the balance tilted towards potentiation ( $+\delta$ ), we see a similar result to that for  $p$  on the invariant set; the unstable manifold is at negative motif strengths (Fig. 8B). Can the motif strengths achieve negative values? Two of them,  $q^{\text{div}}$  and  $q^{\text{con}}$ , are respectively proportional to the variances of neurons' weighted out- and in-degrees. (This can be seen by taking the definitions of these motifs, Eq. (5), and first summing over the indices  $ij$ ). So like the mean connection strength,  $q^{\text{div}}, q^{\text{con}} \geq 0$  and these motifs will always potentiate with this type of STDP rule (Fig. 8B). Chain motifs, in contrast, correspond to the covariance of neurons' weighted in- and out-degrees and so can achieve negative values. Indeed, we see that the strength of chains can depress below zero even while the mean connection strength and other motifs are potentiating (Fig. 5G,A). So with the  $\delta < 0$  balanced STDP rule, since  $q^{\text{ch}}$  decreases, neurons tend to either receive or make many synapses but not both. With the  $\delta > 0$  balanced STDP rule, on the other hand,  $q^{\text{ch}}$  increases along with  $q^{\text{con}}$  and  $q^{\text{div}}$  (Figs. 8B, 9C,D) so that individual neurons tend to become both in- and out-hubs.

Many studies have examined how STDP affects either feedforward or recurrent structure in neuronal networks, commonly showing that STDP promotes feedforward structure at the expense of recurrent loops [32, 52, 53]. This is consistent with the intuition gained from isolated pairs of neurons, where STDP

can induce competition between reciprocal synapses [20]. Our theory provides a new way to examine how STDP regulates feedforward vs recurrent motifs by examining the dynamics of  $q^{\text{ch}}$ . This variable includes both feedforward chains and recurrent loops ( $i = k$  and  $i \neq k$ , respectively, in the definition of  $q^{\text{ch}}$ , Eq. (5)). In order to understand the contribution of each of these to overall potentiation or depression of chains, we break chains up into recurrent loops and feedforward chains:

$$\begin{aligned} q^{\text{rec}} &= \frac{1}{N^3} \sum_{i,j,k} \delta_{ik} \mathbf{W}_{ij} \mathbf{W}_{jk} = \frac{1}{N^3} \sum_{i,j} \mathbf{W}_{ij} \mathbf{W}_{ji} \\ q^{\text{ff}} &= \frac{1}{N^3} \sum_{i,j,k} (1 - \delta_{ik}) \mathbf{W}_{ij} \mathbf{W}_{jk} - p^2 \end{aligned} \quad (13)$$

so  $q^{\text{ch}} = q^{\text{rec}} + q^{\text{ff}}$ . Similarly to for the other second-order motifs, the leading order dynamics of the recurrent motif are:

$$\frac{1}{2\epsilon} \frac{dq^{\text{rec}}}{dt} = r^2 S p_0 (q_X^{\text{rec}} + p p_0) + S_F q^{\text{rec}} + S_B q_{X2}^{\text{rec}} \quad (14)$$

We obtain the dynamics of the feedforward motif by subtracting  $dq^{\text{rec}}/dt$  from  $dq^{\text{ch}}/dt$  (Eq. (49)). The new auxiliary variable  $q_{X2}^{\text{rec}}$  is proportional to the conditional second moment of weights that are part of loops (Eq. (46), and evolves according to Eq. (48). This decomposition imposes a competition between loops and feedforward motifs, but only for a fixed value of  $q^{\text{ch}}$ , since the sum of  $q^{\text{rec}} + q^{\text{ff}}$  would then be conserved. However, as the strength of chains varies, the competition between recurrent and feedforward motifs is less straightforward. We investigate the joint dynamics of feedforward and recurrent motifs by examining how each varies with the strength of chains, freezing all other variables at their initial conditions. Tracking feedforward and recurrent motifs extends the motif theory to 12 dimensions (the original 9, plus  $q^{\text{rec}}$ ,  $q^{\text{ff}}$  and the auxiliary variable  $q_{X2}^{\text{rec}}$ ). Since the full dynamics may not necessarily follow what is predicted in this slice of the motif space, we also examine how the motifs evolve in simulations of a full spiking network.

For depression-dominated balanced STDP ( $\delta < 0$ ), we see that feedforward and recurrent motifs only compete when chains are sufficiently strong in the network so that they overall potentiate. If the chain motif is depressing, however, we see a transient competition between recurrent and feedforward motifs but they then both depress (Fig. 9A,B). For potentiation-dominated balanced STDP ( $\delta > 0$ ), we see the opposite. When chain motifs are overall depressing, feedforward structure potentiates while recurrent loops depress. When chain motifs are overall potentiating, both feedforward and recurrent motifs potentiate. Overall, examining the dynamics of recurrent or feedforward motifs along with the total strength of chains gives accurate predictions of the motif dynamics even when keeping all other variables frozen. After a sufficiently long time, however, the motifs diverge from the picture in the initial slice through the motif space (Fig. 9C,D), since they are coupled to the 9-dimensional motif system.

## Discussion

We have developed a theory for spike timing-dependent plasticity in recurrent networks of integrate-and-fire neurons, which gives accurate predictions for the dynamics of each synaptic weight in the network. We then used this to derive a low-dimensional theory for the plasticity of two-synapse motifs, providing the first theory of motif plasticity in neuronal networks. The form of this theory naturally separates the parameters of the STDP rule into two broad regions: 1) rate-dominated rules with an imbalance between potentiation and depression, and 2) rules with balanced potentiation and depression in which different sources of spike-train covariability interact with the shape of the STDP rule to determine network structure. In the latter case, any mechanism controlling spike-train covariability in the network may have a strong effect on how the network structure evolves. Spike initiation dynamics [54–57], spike-frequency adaptation [58, 59], synaptic inhibition [60–62] and passive membrane properties [63] could all, in addition to controlling firing rates, play a role in shaping correlation-driven motif plasticity.

### STDP in recurrent networks

A recent suite of studies derived a theory for how STDP shapes the full structure of networks of Poisson neurons [31, 38–41, 49]. These studies mostly focused on the effects of training, considering how feedforward inputs entrain structure in the recurrent synapses [?, 31, 40, 49]. In those studies, the only source of spike-time covariability was the input correlation. In contrast, we consider the case where the intrinsic variability of neurons’ spike trains are the only source of spiking covariability. While two studies also examined STDP in networks without training stimuli [38, 39], these took a large system size limit and neglected spike-time correlations. As can be seen in our motif theory, this assumption can be accurate when the STDP is unbalanced – as was indeed the case in these studies. If there is a balance between potentiation and depression, however, the spike-time covariances play a strong role in the plasticity. Furthermore, our use of integrate-and-fire models allows our theory to predict the evolution of network structure without fixing the statistics of individual or joint spiking activity.

### Plasticity of motifs

Many computational studies have asked how STDP affects the structure and activity of recurrent networks [33, 64–66], commonly examining the emergence of highly connected clusters. Early studies focused on isolated pairs of reciprocally connected neurons, showing that the type of STDP we study tends to induce competition between reciprocal synapses (Fig. 1B,C; [20]). Theoretical results on how STDP shapes network-level structure have been difficult to come by. Most studies have examined the average synaptic weight in a network [67, 68], focussing on the relationship between network-averaged firing rates and mean synaptic weights ( $p$ ) but neglecting spike-time correlations. Mean-field theories are accurate for fully homogenous networks. It is straightforward to see, however, that if all neurons have the same weighted in- and out-degrees, then there is no plasticity of two-synapse motifs (Supplemental Information: Motif plasticity in homogenous networks). So plasticity of higher-order networks structure depends on inhomogeneities in neurons’ inputs and outputs.

Most theoretical studies of STDP and network structure have focused on the question of how STDP controls feedforward chains versus recurrent loops. One compared the mean strengths of feedforward versus recurrent inputs in a network receiving synchronous stimulation [53], but did this for a neuron which made no feedback connections to the network – effectively only taking into account the first term of Eq. (7). Another study examined the strength of loops of all lengths in a network of linear, excitatory neurons, showing that STDP tends to reduce the total amounts of loops (across all lengths) in a network [52]. Our theory is restricted to two-synapse loops; while we have shown that these can potentiate (as in Fig.

9C), [52] predicts that longer loops will meanwhile be weakened. The question of how the underlying structure of the network’s adjacency matrix controls the STDP of motifs is ripe for investigation.

## Stability of learned network structures

Early studies of long-term plasticity, which gave rise to the phenomenological plasticity model we used, focused on the relative timing of action potentials. More recent experiments have shown that neurons’ firing rates and the postsynaptic membrane voltage and spike patterns all affect the shape of measured STDP curves [51, 69–72]. More complicated models of long-term plasticity, based on spike-triplet- or voltage-dependent STDP [73, 74] or on calcium thresholds for the induction of depression and potentiation [75–77], can replicate many of these complexities. The observation that firing rates undergo large fluctuations over slow timescales [78–82] suggests that STDP also transitions between unbalanced potentiation- and depression-dominated regimes. While long-term plasticity can be strongly affected by pre- and post-synaptic firing rates, the motif structure and shape of spike-train correlations could determine the direction of network-level plasticity during transitions between potentiation- and depression-dominated regimes.

A major feature of STDP is that it can potentiate temporally correlated inputs [29]. Since synchronous inputs are effective at driving postsynaptic spiking, this can give rise to pathological activity in recurrent networks [34]. Synaptic depression driven by postsynaptic spikes, independent of presynaptic activity, can stabilize postsynaptic firing rates during STDP [25, 31]. Such additional rate-dependent terms of the plasticity rule can also stabilize the full weight matrix [39], and so could give rise to stable motif configurations. Recent work has focused on the necessity of homeostatic mechanisms, including synaptic scaling [83] or inhibitory plasticity, in stabilizing both the activity and structure of neural networks [32, 36, 84–87]. Since balanced STDP can give rise to bistability of mean synaptic weights in a network (Fig. 7B), balanced STDP could also provide a mechanism for assembly formation, suggesting that homeostatic mechanisms could have the effect of balancing potentiation and depression.

The additive, Hebbian STDP model we used here gives rise to splitting of synaptic weights: individual weights potentiate to some upper bound, or depress away completely. This gives rise to bimodal distributions of synaptic weights, while experimentally observed weight distributions tend to be unimodal and long-tailed [?, 3, 4, 88]. Simple modifications of this model, such as introducing axonal or dendritic delays or weight-dependence of plasticity, can yield weight distributions more closely resembling those observed in neural tissue [26–28, 89, 90]. Strong weight dependence, however, forces every weight to the same value so that the baseline motif frequencies completely determine the structure of the weight matrix (Supplemental Information: Multiplicative STDP). The dynamics of motifs under more realistic models of synaptic plasticity remain to be studied.

## Methods

### Neuron and network model

We model a network of  $N$  neurons. The membrane dynamics of individual neurons obey the exponential integrate-and-fire (EIF) model [45], one of a class of models well-known to capture the spike initiation dynamics and statistics of cortical neurons [46,47]. Specifically, the membrane voltage of neuron  $i$  evolves according to:

$$C \frac{dV_i}{dt} = g_L (V_L - V_i) + g_L \Delta \exp\left(\frac{V_i - V_T}{\Delta}\right) + I_i(t) + \sum_{j=1}^N \mathbf{W}_{ij} (\mathbf{J}_{ij} * y_j). \quad (15)$$

The first term on the right-hand side is the leak current, with conductance  $g_L$  and reversal potential  $V_L$ . The next term describes a phenomenological action potential with an initiation threshold  $V_T$  and steepness  $\Delta$ : when the voltage reaches  $V_T$ , it diverges; this divergence marks an action potential. For numerical simulations, action potentials are thresholded at  $V(t) = V_{\text{th}}$ , reset to a reset potential  $V_{re}$  and held there for an absolute refractory period  $\tau_{\text{ref}}$ .

Input from external sources not included in the model network is contained in  $I_i(t)$ . We model this as a Gaussian white noise process:  $I_i(t) = \mu + g_L \sigma D \xi_i(t)$ . The mean of the the external input current is  $\mu$ . The parameter  $\sigma$  controls the strength of the noise and  $D = \sqrt{\frac{2C}{g_L}}$  scales the noise amplitude to be independent of the passive membrane time constant. With this scaling, the infinitesimal variance of the passive membrane voltage is  $(g_L \sigma D)^2$ .

The last term of Eq. (15) models synaptic interactions in the network. The  $N \times N$  matrix  $\mathbf{W}$  contains the amplitudes of each synapse's postsynaptic currents. It is a weighted version of the binary adjacency matrix  $\mathbf{W}^0$ , where  $\mathbf{W}_{ij}^0 = 1(0)$  indicates the presence (absence) of a synapse from neuron  $j$  onto neuron  $i$ . If a synapse  $ij$  is present then  $\mathbf{W}_{ij}$  denotes its strength. Due to synaptic plasticity,  $\mathbf{W}$  is dynamic; it changes in time as individual synapses potentiate or depress. The spike train from neuron  $j$  is the point process  $y_j(t) = \sum_k \delta(t - t_j^k)$ , where  $t_j^k$  denotes the  $k^{\text{th}}$  spike time from neuron  $j$ . The  $N \times N$  matrix  $\mathbf{J}(t)$  defines the shape of the post-synaptic currents. In this study, we use exponential synapses:  $\mathbf{J}_{ij}(t - t_j^k) = \mathcal{H}(t - t_j^k) \exp\left(-\frac{t - t_j^k}{\tau_s}\right)$ , where  $\mathcal{H}(t)$  is the Heaviside step function. Our theory is not exclusive to the EIF model or to the simple synaptic kernels we used; similar methods can be used with any integrate-and-fire model and arbitrary synaptic kernels. Model parameters are contained in Table 1 (unless specified otherwise in the text).

The baseline structure of the network is defined by the adjacency matrix  $\mathbf{W}^0$ . The frequencies of different motifs are:

$$\begin{aligned} p_0 &= \frac{1}{N^2} \sum_{i,j} \mathbf{W}_{ij}^0, \\ q_0^{\text{div}} &= \frac{1}{N^3} \sum_{i,j,k} \mathbf{W}_{ik}^0 \mathbf{W}_{jk}^0 - p_0^2, \\ q_0^{\text{con}} &= \frac{1}{N^3} \sum_{i,j,k} \mathbf{W}_{ik}^0 \mathbf{W}_{ij}^0 - p_0^2, \\ q_0^{\text{ch}} &= \frac{1}{N^3} \sum_{i,j,k} \mathbf{W}_{ij}^0 \mathbf{W}_{jk}^0 - p_0^2. \end{aligned} \quad (16)$$

Each of the  $q_0$  parameters refers to a different two-synapse motif. In divergent motifs ( $q_0^{\text{div}}$ ), one neuron  $k$  projects to two others,  $i$  and  $j$ . In convergent motifs, two neurons  $k$  and  $j$  project to a third,  $i$ . In chain motifs, neuron  $k$  projects to neuron  $j$ , which projects to neuron  $i$ . In each of these equations, we subtract off  $p_0^2$  to correct for the baseline frequencies expected in Erdős-Rényi random networks. So, these parameters measure above-chance levels of motif structure in the adjacency matrix  $\mathbf{W}^0$ .

## Learning dynamics

We now derive Eq. (2), summarizing a key result of [29]. Changes in a synaptic weight  $\mathbf{W}_{ij}$  are governed by the learning rule  $L(s)$ , Eq. (1). We begin by considering the total change in synaptic weight during an interval of length  $T$  ms:

$$\Delta \mathbf{W}_{ij} = \mathbf{W}_{ij}^0 \int_t^{t+T} \int_t^{t+T} L(t'' - t') y_j(t'') y_i(t') dt'' dt' \quad (17)$$

where multiplying by the corresponding element of the adjacency matrix ensures that nonexistent synapses do not potentiate into existence. Consider the trial-averaged rate of change:

$$\frac{\langle \Delta \mathbf{W}_{ij} \rangle}{T} = \mathbf{W}_{ij}^0 \frac{1}{T} \int_t^{t+T} \int_{t-t'}^{t+T-t'} L(s) \langle y_j(t' + s) y_i(t') \rangle ds dt' \quad (18)$$

where  $s = t'' - t'$  and  $\langle \cdot \rangle$  denotes the trial average. We first note that this contains the definition of the trial-averaged spike train cross-covariance:

$$\mathbf{C}_{ij}(s) = \frac{1}{T} \int_t^{t+T} \langle y_j(t' + s) y_i(t') \rangle dt' - r_i r_j \quad (19)$$

where  $r_i$  is the time-averaged firing rate of neuron  $i$  and subtracting off the product of the rates corrects for chance spike coincidences. Inserting this definition into Eq. (18) yields:

$$\frac{\langle \Delta \mathbf{W}_{ij} \rangle}{T} = \mathbf{W}_{ij}^0 \int_{t-t'}^{t+T-t'} L(s) (r_i r_j + \mathbf{C}_{ij}(s)) ds \quad (20)$$

We then take the amplitude of individual changes in the synaptic weights to be small:  $f_+, f_- \ll W^{\text{max}}$ , where  $\tau_{\pm}$  define the temporal shape of the STDP rule (see Eq. (1)). In this case, changes in the weights occur on a slower timescale than the width of the learning rule. Taking  $T \gg \max(\tau_+, \tau_-)$  allows us to extend the limits of integration in Eq. (20) to  $\pm\infty$ , which gives Eq. (2). Note that in the results we have dropped the angle brackets for convenience. This can also be justified by the fact that the plasticity is self-averaging, since  $\Delta \mathbf{W}_{ij}$  depends on the integrated changes over the period  $T$ .

## Spiking statistics

In order to calculate  $d\mathbf{W}_{ij}/dt$ , we need to know the firing rates  $r_i, r_j$  and spike train cross-covariance  $\mathbf{C}_{ij}(s)$  (Eq. (2)). We take the weights to be constant on the fast timescale of  $s$ , so that the firing rates and spike train cross-covariances are stationary on that timescale. We solve for the baseline firing rates in the network via the self-consistency relationship

$$r_i = r_i(\mu_i^{\text{eff}}, \sigma), \text{ where}$$

$$\mu_i^{\text{eff}} = \mu + \sum_j \left( \int_{-\infty}^{\infty} \mathbf{J}_{ij}(t) dt \right) \mathbf{W}_{ij} r_j$$

for  $i = 1, \dots, N$ . This gives the equilibrium state of each neuron's activity. In order to calculate the spike train cross-covariances, we must consider temporal fluctuations around the baseline firing rates.

With sufficiently weak synapses compared to the background input, we can linearize each neuron's activity around the baseline state. Rather than linearizing each neuron's firing rate around  $r_i$ , we follow [13, 42, 43] and linearize each neuron's spike train around a realization of background activity, the uncoupled spike train  $\mathbf{y}_i^0$  (Eq. (3)). The perturbation around the background activity is given by each neuron's linear response function,  $\mathbf{A}_i(t)$ , which measures the amplitude of firing rate fluctuations in response to perturbations of each neuron's input around the baseline  $\mu_{eff}$ . We calculate  $\mathbf{A}(t)$  using standard methods based on Fokker-Planck theory for the distribution of a neuron's membrane potential [91, 92].

This yields Eq. (3), approximating a realization of each neuron's spike train as a mixed point and continuous process. Spike trains are defined, however, as pure point processes. Fortunately, Eq. (2) shows that we do not need a prediction of individual spike train realizations, but rather of the trial-averaged spiking statistics. We can solve Eq. (3) for the spike trains in the frequency domain as:

$$\mathbf{y}(\omega) = (\mathbf{I} - (\mathbf{W} \cdot \mathbf{K}(\omega)))^{-1} \mathbf{y}^0(\omega)$$

where as in the Results,  $\mathbf{K}(\omega)$  is an interaction matrix defined by  $\mathbf{K}_{ij}(\omega) = \mathbf{A}_i(\omega) \mathbf{J}_{ij}(\omega)$  and  $\cdot$  denotes the element-wise product. Averaging this expression over realizations of the background spike trains yields a linear equation for the instantaneous firing rates. Averaging the spike trains  $\mathbf{y}$  against each other yields the full cross-covariance matrix, Eq. (4). It depends on the coupling strengths  $\mathbf{W}$ , the synaptic filters  $\mathbf{J}_{ij}$  and neurons' linear response functions  $\mathbf{A}$ , and the covariance of the baseline spike trains,  $\mathbf{C}^0$ .

We can calculate the baseline covariance in the frequency domain,  $\mathbf{C}^0(\omega) = \langle \mathbf{y}^0 \mathbf{y}^{0*} \rangle$ , by first noting that it is a diagonal matrix containing each neuron's spike train power spectrum. We calculate these using the renewal relationship between the spike train power spectrum  $\mathbf{C}^0(\omega)$  and the first passage time density [93]; the first passage time density for nonlinear integrate and fire models can be calculated using similar methods as for the linear response functions [92].

## Self-consistent theory for network plasticity

We solve the system Eqs. (2),(4) for the evolution of each synaptic weight with the Euler method with a time step of 100 seconds. A package of code for solving the self-consistent theory and running the spiking simulations, in MATLAB and C, is available at <http://sites.google.com/site/gabrielkochocker/code>. Additional code is available on request.

## Derivation of motif plasticity

The mean synaptic weight and the definitions of the two-synapse motifs are given by Eqs. (5). Since our linear response theory for synaptic plasticity requires weak synapses, here we explicitly scale by the mean in-degree  $\epsilon = \frac{1}{N p_0}$ :



$$\begin{aligned}
\epsilon p &= \frac{1}{N^2} \sum_{i,j} \mathbf{W}_{ij}, \\
\epsilon^2 q^{\text{div}} &= \frac{1}{N^3} \sum_{i,j,k} \mathbf{W}_{ik} \mathbf{W}_{jk} - \epsilon^2 p^2, \\
\epsilon^2 q^{\text{con}} &= \frac{1}{N^3} \sum_{i,j,k} \mathbf{W}_{ik} \mathbf{W}_{ij} - \epsilon^2 p^2, \\
\epsilon^2 q^{\text{ch}} &= \frac{1}{N^3} \sum_{i,j,k} \mathbf{W}_{ij} \mathbf{W}_{jk} - \epsilon^2 p^2, \\
\epsilon q_X^{\text{rec}} &= \frac{1}{N^2} \sum_{i,j} \mathbf{W}_{ij} \mathbf{W}_{ji}^0 - \epsilon p p_0, \\
\epsilon q_X^{\text{div}} &= \frac{1}{N^3} \sum_{i,j,k} \mathbf{W}_{ik} \mathbf{W}_{jk}^0 - \epsilon p p_0, \\
\epsilon q_X^{\text{con}} &= \frac{1}{N^3} \sum_{i,j,k} \mathbf{W}_{ik} \mathbf{W}_{ij}^0 - \epsilon p p_0, \\
\epsilon q_X^{\text{ch,A}} &= \frac{1}{N^3} \sum_{i,j,k} \mathbf{W}_{ij} \mathbf{W}_{jk}^0 - \epsilon p p_0, \\
\epsilon q_X^{\text{ch,B}} &= \frac{1}{N^3} \sum_{i,j,k} \mathbf{W}_{ij}^0 \mathbf{W}_{jk} - \epsilon p p_0
\end{aligned} \tag{21}$$

Here we have defined the two-synapse motifs, as well as five auxiliary variables,  $\{q_X\}$ . These mixed motifs, defined by products of the weight and adjacency matrices, measure the strength of synapses *conditioned* on their being part of a motif. The motifs  $\{q\}$ , on the other hand, measure the total strength of the motifs. While the variables  $\{q_X\}$  are not of direct interest, we will see that they are required in order to close the system of equations. In comparison to the motif *frequencies*  $\{q_0\}$ , which measure motif frequencies in comparison to an independently *connected* network, the motif *strengths* are defined relative to an independently *weighted* network.

We also scale the amplitude of individual synaptic changes,  $L(s)$ , by  $\epsilon$ . We now go through the derivation of  $dp/dt$ ,  $dq^{\text{div}}/dt$  and  $dq_X^{\text{div}}/dt$  as examples; the other six variables follow the same steps. First, note that the spike train cross-covariance matrix of the network, Eq. (4), can be expanded in the Fourier domain around the baseline covariance  $\mathbf{C}^0(\omega)$ :

$$\mathbf{C}(\omega) = \left( \sum_{i=0}^{\infty} (\mathbf{W} \cdot \mathbf{K})^i \right) \mathbf{C}^0(\omega) \left( \sum_{j=0}^{\infty} ((\mathbf{W} \cdot \mathbf{K})^*)^j \right) \tag{22}$$

where the interaction matrix  $\mathbf{W} \cdot \mathbf{K}$  is the element-wise product of the weight matrix  $\mathbf{W}$  and the matrix of filters,  $\mathbf{K}$ . Powers of  $\mathbf{W} \cdot \mathbf{K}$  represent path lengths through the network. Only taking into account up to length one paths yields (for  $i \neq j$ ):

$$\mathbf{C}_{ij}(s) \approx \underbrace{(\mathbf{W}_{ij} \mathbf{K}_{ij} * \mathbf{C}_{jj}^0)}_{\text{forward connection}}(s) + \underbrace{(\mathbf{C}_{ii}^0 * \mathbf{W}_{ji} \mathbf{K}_{ji}^-)}_{\text{backward connection}}(s) + \underbrace{\sum_k (\mathbf{W}_{ik} \mathbf{K}_{ik} * \mathbf{C}_{kk}^0 * \mathbf{W}_{jk} \mathbf{K}_{jk}^-)}_{\text{common inputs}}(s). \tag{23}$$

where we have inverse Fourier transformed for convenience in the following derivation and  $\mathbf{K}^-(t) = \mathbf{K}(-t)$ .

Differentiating each motif with respect to time, using the slow-fast STDP theory Eq. (2) and inserting the first-order truncation of the cross-covariance functions, Eq. (7), yields:

$$\begin{aligned} \epsilon \frac{dp}{dt} &= \frac{1}{N^2} \sum_{i,j} \mathbf{W}_{ij}^0 \int_{-\infty}^{\infty} \epsilon L(s) \left( r_i r_j + \delta_{ij} \mathbf{C}_{ij}^0(s) + (\mathbf{W}_{ij} \mathbf{K}_{ij} * \mathbf{C}_{jj}^0)(s) \right. \\ &\quad \left. + (\mathbf{C}_{ii}^0 * \mathbf{W}_{ji} \mathbf{K}_{ji}^-)(s) + \sum_k \left( \mathbf{W}_{ik} \mathbf{K}_{ik} * \mathbf{C}_{kk}^0 * \mathbf{W}_{jk} \mathbf{K}_{jk}^- \right) \right) ds \end{aligned} \quad (24)$$

$$\begin{aligned} \epsilon^2 \frac{dq^{\text{div}}}{dt} &= \frac{2}{N^3} \sum_{i,j,k} \left[ \mathbf{W}_{ik} \mathbf{W}_{jk}^0 \int_{-\infty}^{\infty} \epsilon L(s) \left( r_j r_k + \delta_{jk} \mathbf{C}_{jk}^0(s) + (\mathbf{W}_{jk} \mathbf{K}_{jk} * \mathbf{C}_{kk}^0)(s) \right. \right. \\ &\quad \left. \left. + (\mathbf{C}_{jj}^0 * \mathbf{W}_{kj} \mathbf{K}_{kj}^-)(s) + \sum_l \left( \mathbf{W}_{jl} \mathbf{K}_{jl} * \mathbf{C}_{ll}^0 * \mathbf{W}_{kl} \mathbf{K}_{kl}^- \right) \right) ds \right] - 2\epsilon^2 p \frac{dp}{dt} \end{aligned} \quad (25)$$

$$\begin{aligned} \epsilon \frac{dq_X^{\text{div}}}{dt} &= \frac{1}{N^3} \sum_{i,j,k} \mathbf{W}_{jk}^0 \mathbf{W}_{ik}^0 \int_{-\infty}^{\infty} \epsilon L(s) \left( r_i r_k + \delta_{ik} \mathbf{C}_{ik}^0(s) + (\mathbf{W}_{ik} \mathbf{K}_{ik} * \mathbf{C}_{kk}^0)(s) \right. \\ &\quad \left. + (\mathbf{C}_{ii}^0 * \mathbf{W}_{ki} \mathbf{K}_{ki}^-)(s) + \sum_l \left( \mathbf{W}_{il} \mathbf{K}_{il} * \mathbf{C}_{ll}^0 * \mathbf{W}_{kl} \mathbf{K}_{kl}^- \right) \right) ds \Big] - \epsilon p_0 \frac{dp}{dt} \end{aligned} \quad (26)$$

We now assume that all neurons have the same firing rates, spike train autocovariances and linear response functions:  $\forall i, r_i \equiv r$ ,  $\mathbf{C}_{ii}^0 \equiv C^0$  and  $\mathbf{A}_i \equiv A$ . Since we model all post-synaptic currents with the same shape, this makes the matrix  $\mathbf{K}$  a constant matrix; we replace its elements with the scalar  $K$ . Also neglecting the weight bounds in  $L(s)$  allows us to write:

$$\frac{dp}{dt} = r^2 S \frac{1}{N^2} \sum_{i,j} \mathbf{W}_{ij}^0 + S_F \frac{1}{N^2} \sum_{i,j} \mathbf{W}_{ij}^0 \mathbf{W}_{ij} + S_B \frac{1}{N^2} \sum_{i,j} \mathbf{W}_{ij}^0 \mathbf{W}_{ji} + S_C \frac{1}{N^2} \sum_{i,j,k} \mathbf{W}_{ij}^0 \mathbf{W}_{ik} \mathbf{W}_{jk} \quad (27)$$

$$\begin{aligned} \frac{dq^{\text{div}}}{dt} &= r^2 S \frac{2}{N^3} \sum_{i,j,k} \mathbf{W}_{ik} \mathbf{W}_{jk}^0 + S_F \frac{2}{N^3} \sum_{i,j,k} \mathbf{W}_{ik} \mathbf{W}_{jk}^0 \mathbf{W}_{jk} \\ &\quad + S_B \frac{2}{N^3} \sum_{i,j,k} \mathbf{W}_{ik} \mathbf{W}_{jk}^0 \mathbf{W}_{kj} + S_C \frac{2}{N^3} \sum_{i,j,k,l} \mathbf{W}_{ik} \mathbf{W}_{jk}^0 \mathbf{W}_{jl} \mathbf{W}_{kl} - 2\epsilon p \frac{dp}{dt} \end{aligned} \quad (28)$$

$$\begin{aligned} \frac{dq_X^{\text{div}}}{dt} &= r^2 S \frac{1}{N^3} \sum_{i,j,k} \mathbf{W}_{jk}^0 \mathbf{W}_{ik}^0 + S_F \frac{1}{N^3} \sum_{i,j,k} \mathbf{W}_{jk}^0 \mathbf{W}_{ik}^0 \mathbf{W}_{ik} \\ &\quad + S_B \frac{1}{N^3} \sum_{i,j,k} \mathbf{W}_{jk}^0 \mathbf{W}_{ik}^0 \mathbf{W}_{ki} + S_C \frac{1}{N^3} \sum_{i,j,k,l} \mathbf{W}_{jk}^0 \mathbf{W}_{ik}^0 \mathbf{W}_{il} \mathbf{W}_{kl} - p_0 \frac{dp}{dt} \end{aligned} \quad (29)$$

where we have cancelled off an  $\epsilon$  from the left and right-hand sides. We have absorbed the integrals over the STDP rule and the spike-train covariances into  $r^2 S$ ,  $S_F$ ,  $S_B$  and  $S_C$ . These correspond, respectively, to the total STDP-weighted spike-train covariances from chance coincidence, forward connections, backward connections, and common input:

$$S = \int_{-\infty}^{\infty} L(s) ds \quad (30)$$

$$S_F = \int_{-\infty}^{\infty} L(s) (K(t) * C^0(s)) ds \quad (31)$$

$$S_B = \int_{-\infty}^{\infty} L(s) (C^0(s) * K^-(t)) ds \quad (32)$$

$$S_C = \int_{-\infty}^{\infty} L(s) (K(t) * C^0(s) * K^-(t)) ds \quad (33)$$

These parameters depend on the spike train auto-covariance  $C^0(s)$  and linear response functions  $A(t)$  of neurons. These functions can change as the network's operating point does; for instance, as the leak reversal  $V_L$  increases, neurons will shift to a mean-driven, more oscillatory spiking regime and  $C^0(s)$  and  $K(t; A)$  will change. As the mean synaptic weight changes, the firing rates will change and this can also affect  $C^0(s)$  and  $K(t; A)$ . We have assumed weak synapses, so we will fix these at their value at  $p = p_0 W^{\max}/2$ . Without this approximation, the system is transcendental.

Each dynamical equation now contains four different sums of products of the weight and adjacency matrices. First examining  $dp/dt$ , we see that the first three sums correspond to defined motifs:  $1/N^2 \sum_{i,j} \mathbf{W}_{ij}^0 = p_0$ ,  $1/N^2 \sum_{i,j} \mathbf{W}_{ij}^0 \mathbf{W}_{ij} = p$  and  $1/N^2 \sum_{i,j} \mathbf{W}_{ij}^0 \mathbf{W}_{ji} = q_X^{\text{rec}} + pp_0$ . The last term in Eq. (27), however, corresponds to a third-order motif mixed between the weight and adjacency matrices. Similarly, third- and fourth-order mixed motifs appear in Eqs. 28 and 29. In order to calculate these, we extend a re-summing technique developed in [14]. We assume that there are no third- or higher-order correlations between elements of the weight and/or adjacency matrices, and approximate the frequency of each of these higher-order motifs by the number of ways it can be composed of one and two-synapse motifs. For a third order motif, this corresponds to adding up the likelihoods that all three synapses occur by chance and that each possible combination of one synapse and a two-synapse motif occur. In Eq. (27), for example:

$$\sum_{i,j,k} \mathbf{W}_{ij}^0 \mathbf{W}_{ik} \mathbf{W}_{jk} \approx \epsilon^2 N^3 \left( p_0 (q^{\text{div}} + p^2) + p (q_X^{\text{con}} + q_X^{\text{ch,B}}) \right). \quad (34)$$

and for the four-synapse motif in Eq. (28),

$$\sum_{i,j,k,l} \mathbf{W}_{ik} \mathbf{W}_{jk}^0 \mathbf{W}_{jl} \mathbf{W}_{kl} \approx \epsilon^3 N^4 \left( p^3 p_0 + p^2 (q_X^{\text{div}} + q_X^{\text{con}} + q_X^{\text{ch,B}}) + pp_0 (q^{\text{div}} + q^{\text{ch}}) + q^{\text{div}} q_X^{\text{div}} + q^{\text{ch}} q_X^{\text{con}} \right) \quad (35)$$

This re-summing, along with the inclusion of the mixed motifs  $\{q_X\}$ , is what allows us to close the motif dynamics. Re-summing each third- and fourth-order motif in our system in terms of two-synapse motifs yields, after simplification, the final motif dynamics:

$$\frac{dp}{dt} = p_0 r^2 S + \epsilon \left[ p S_F + (q_X^{\text{rec}} + p_0 p) S_B + \frac{1}{p_0} \left( p_0 (q^{\text{div}} + p^2) + p (q_X^{\text{con}} + q_X^{\text{ch,B}}) \right) S_C \right] \quad (36)$$

$$\frac{dq^{\text{div}}}{dt} = 2r^2 S q_X^{\text{div}} + 2\epsilon \left[ q^{\text{div}} S_F + (p_0 q^{\text{ch}} + p q_X^{\text{div}}) S_B + \frac{1}{p_0} (q^{\text{ch}} (q_X^{\text{con}} + pp_0) + q_X^{\text{div}} (q^{\text{div}} + p^2)) S_C \right] \quad (37)$$

$$\frac{dq^{\text{con}}}{dt} = 2r^2 S q_X^{\text{con}} + 2\epsilon \left[ q^{\text{con}} S_F + (p_0 q^{\text{ch}} + p q_X^{\text{con}}) S_B + \frac{1}{p_0} (q^{\text{con}} (q_X^{\text{ch,B}} + pp_0) + q_X^{\text{con}} (q^{\text{div}} + p^2)) S_C \right] \quad (38)$$

$$\begin{aligned} \frac{dq^{\text{ch}}}{dt} &= r^2 S (q_X^{\text{ch,A}} + q_X^{\text{ch,B}}) + \epsilon \left[ 2q^{\text{ch}} S_F + (p_0 (q^{\text{con}} + q^{\text{div}}) + p (q_X^{\text{ch,A}} + q_X^{\text{ch,B}})) S_B \right. \\ &\quad \left. + \frac{1}{p_0} (q_X^{\text{ch,A}} (q^{\text{div}} + p^2) + q_X^{\text{ch,B}} (q^{\text{div}} + q^{\text{con}} + p^2)) S_C \right] \end{aligned} \quad (39)$$

$$\begin{aligned} \frac{dq_X^{\text{rec}}}{dt} &= r^2 S q_0^{\text{rec}} + \epsilon \left[ q_X^{\text{rec}} S_F + (1 - p_0) (q_X^{\text{rec}} + pp_0) S_B \right. \\ &\quad \left. + \frac{1}{p_0} (q_0^{\text{rec}} (q^{\text{div}} + p^2) + q_X^{\text{ch,B}} (q_X^{\text{ch,B}} + pp_0) + q_X^{\text{con}} (q_X^{\text{con}} + pp_0)) S_C \right] \end{aligned} \quad (40)$$

$$\frac{dq_X^{\text{div}}}{dt} = r^2 S q_0^{\text{div}} + \epsilon \left[ q_X^{\text{div}} S_F + \left( p q_0^{\text{div}} + p_0 q_X^{\text{ch,B}} \right) S_B + \frac{1}{p_0} \left( q_0^{\text{div}} (q^{\text{div}} + p^2) + q_X^{\text{ch,B}} (q_X^{\text{con}} + p p_0) \right) S_C \right] \quad (41)$$

$$\frac{dq_X^{\text{con}}}{dt} = r^2 S q_0^{\text{con}} + \epsilon \left[ q_X^{\text{con}} S_F + \left( p q_0^{\text{con}} + p_0 q_X^{\text{ch,A}} \right) S_B + \frac{1}{p_0} \left( q_0^{\text{con}} (q^{\text{div}} + p^2) + q_X^{\text{con}} (q_X^{\text{ch,B}} + p p_0) \right) S_C \right] \quad (42)$$

$$\frac{dq_X^{\text{ch,A}}}{dt} = r^2 S q_0^{\text{ch}} + \epsilon \left[ q_X^{\text{ch,A}} S_F + \left( p q_0^{\text{ch}} + p_0 q_X^{\text{con}} \right) S_B + \frac{1}{p_0} \left( q_0^{\text{ch}} (q^{\text{div}} + p^2) + q_X^{\text{con}} (q_X^{\text{con}} + p p_0) \right) S_C \right] \quad (43)$$

$$\frac{dq_X^{\text{ch,B}}}{dt} = r^2 S q_0^{\text{ch}} + \epsilon \left[ q_X^{\text{ch,B}} S_F + \left( p q_0^{\text{ch}} + p_0 q_X^{\text{div}} \right) S_B + \frac{1}{p_0} \left( q_0^{\text{ch}} (q^{\text{div}} + p^2) + q_X^{\text{ch,B}} (q_X^{\text{ch,B}} + p p_0) \right) S_C \right] \quad (44)$$

Examination of these equations reveals how different types of joint spiking activity affect motif dynamics. Chance spiking coincidence (the  $r^2 S$  terms) couple each motif to the mixed version of itself, and each mixed motif to the baseline structure of the adjacency matrix. With Hebbian STDP and excitatory synapses,  $S_F > 0$  and  $S_B < 0$ . So, spiking correlations from forward connections provide positive feedback, reinforcing the current network structure. Spiking correlations from backward connections and common input couple divergent, convergent and chain motifs to each other.

The dynamics on the invariant set (Results: Balanced STDP of the mean synaptic weight, Fig. 7) were plotted in MATLAB. The vector fields of Figs. 8 and 9 were calculated in XPPAUT. For those figures, results from simulations of the full spiking network were plotted in MATLAB and then overlaid on the vector fields from XPPAUT.

### Plasticity of loops and feedforward chains

The chain variable  $q^{\text{ch}}$  includes both feedforward and recurrent loops. (Feedforward chains correspond to  $k \neq i$  in the definition of  $q^{\text{ch}}$ , Eq. (21), and recurrent loops to  $k = i$ .) As in the main text, we break  $q^{\text{ch}}$  into these two cases:  $q^{\text{ch}} = q^{\text{rec}} + q^{\text{ff}}$ , where

$$\begin{aligned} \epsilon^2 q^{\text{rec}} &= \frac{1}{N^3} \sum_{i,j,k} \delta_{ik} \mathbf{W}_{ij} \mathbf{W}_{jk} = \frac{1}{N^3} \sum_{i,j} \mathbf{W}_{ij} \mathbf{W}_{ji} \\ \epsilon^2 q^{\text{ff}} &= \frac{1}{N^3} \sum_{i,j,k} (1 - \delta_{ik}) \mathbf{W}_{ij} \mathbf{W}_{jk} - \epsilon^2 p^2 \end{aligned} \quad (45)$$

We also define an auxiliary variable which we will require in the dynamics of  $q^{\text{rec}}$ :

$$\epsilon^2 q_{X2}^{\text{rec}} = \frac{1}{N^3} \sum_{i,j} \mathbf{W}_{ij}^2 \mathbf{W}_{ij}^0 \quad (46)$$

which is proportional to the conditioned second moment of weights that are part of disynaptic loops. The dynamics of  $q^{\text{rec}}$  are calculated exactly as for the other motifs and are:

$$\frac{1}{2\epsilon} \frac{dq^{\text{rec}}}{dt} = r^2 S p_0 (q_X^{\text{rec}} + p p_0) + S_F q^{\text{rec}} + S_B q_{X2}^{\text{rec}} \quad (47)$$

where the new auxiliary variable obeys

$$\frac{1}{2\epsilon} \frac{dq_{X2}^{\text{rec}}}{dt} = r^2 S p_0 (q_X^{\text{rec}} + p p_0) + S_F q_{X2}^{\text{rec}} + S_B q^{\text{rec}} \quad (48)$$

We can then recover the dynamics of feedforward chains as:

$$\begin{aligned}
\frac{dq^{\text{ff}}}{dt} &= \frac{dq^{\text{ch}}}{dt} - \frac{dq^{\text{rec}}}{dt} \\
&= r^2 S \left( q_X^{\text{ch,A}} + q_X^{\text{ch,B}} \right) + \epsilon \left[ -2r^2 S p_0 (q_X^{\text{rec}} + p p_0) + 2S_F (q^{\text{ch}} - q^{\text{rec}}) \right. \\
&\quad + \left( p_0 (q^{\text{con}} + q^{\text{div}}) + p \left( q_X^{\text{ch,A}} + q_X^{\text{ch,B}} \right) - 2q_{X2}^{\text{rec}} \right) S_B \\
&\quad \left. + \frac{1}{p_0} \left( q_X^{\text{ch,A}} (q^{\text{div}} + p^2) + q_X^{\text{ch,B}} (q^{\text{div}} + q^{\text{con}} + p^2) \right) S_C \right]
\end{aligned} \tag{49}$$

### Unbalanced STDP

When there is an imbalance between the net amounts of potentiation and depression in the STDP rule, the motif dynamics are governed by simpler equations. If  $S \sim \mathcal{O}(1)$ , the  $\mathcal{O}(\epsilon)$  terms in Eqs. 36-44 are negligible. For each mixed motif,

$$q_X(t) = r^2 S q_0 t + q_X(0) \tag{50}$$

so that

$$p(t) = p_0 r^2 S t + p(0) \tag{51}$$

$$q^{\text{div}}(t) = q^{\text{div}}(0) + q_X^{\text{div}}(0) r^2 S t + \frac{1}{2} q_0^{\text{div}} (r^2 S)^2 t^2 \tag{52}$$

$$q^{\text{con}}(t) = q^{\text{con}}(0) + q_X^{\text{con}}(0) r^2 S t + \frac{1}{2} q_0^{\text{con}} (r^2 S)^2 t^2 \tag{53}$$

$$q^{\text{ch}}(t) = q^{\text{ch}}(0) + \left( q_X^{\text{ch,A}}(0) + q_X^{\text{ch,B}}(0) \right) r^2 S t + \frac{1}{2} q_0^{\text{ch}} (r^2 S)^2 t^2 \tag{54}$$

Writing  $q_X^{\text{ch}} = q_X^{\text{ch,A}} + q_X^{\text{ch,B}}$  puts the dynamics for all the motifs in the same form. The motifs expand from the initial conditions and baseline structure of the network. Note that since the quadratic term is proportional to  $S^2$ , even when the STDP is depression-dominated the long-term dynamics are expansive rather than contractive.

### Balanced, temporally symmetric STDP

By balanced STDP, we mean that the total amounts of potentiation and depression in the STDP rule approximately cancel:  $S \sim \mathcal{O}(\epsilon)$ . As discussed in the Results, when the STDP rule is temporally symmetric ( $\tau_+ = \tau_- \equiv \tau$ ), the correlations from forward and backward correlations are related. We write the integral of the STDP rule as  $S = \pm \delta \epsilon \tau$ , so that the balance can be tilted in favor of potentiation or depression. For  $-\delta$ ,  $S_B \approx -(1 + \delta \epsilon) S_F$ . For  $+\delta$ ,  $S_B \approx -S_F / (1 + \delta \epsilon) = -S_F (1 - \delta \epsilon + \mathcal{O}(\epsilon^2)) \approx -S_F (1 - \delta \epsilon)$ . Additionally, since the spike-train correlations from common input are temporally symmetric (Fig. 6),  $S_C \sim \mathcal{O}(\epsilon)$ . With these simplifications, the leading order motif dynamics become:

$$\frac{1}{\epsilon} \frac{dp}{dt} = \pm \delta \tau p_0 r^2 S + (p(1 - p_0) - q_X^{\text{rec}}) S_F \tag{55}$$

$$\frac{1}{\epsilon} \frac{dq^{\text{div}}}{dt} = \pm 2r^2 \delta \tau q_X^{\text{div}} + 2 \left( q^{\text{div}} - (p_0 q^{\text{ch}} + p q_X^{\text{div}}) \right) S_F \tag{56}$$

$$\frac{1}{\epsilon} \frac{dq^{\text{con}}}{dt} = \pm 2r^2 \delta \tau q_X^{\text{con}} + 2 \left( q^{\text{con}} - (p_0 q^{\text{ch}} + p q_X^{\text{con}}) \right) S_F \tag{57}$$

$$\frac{1}{\epsilon} \frac{dq^{\text{ch}}}{dt} = \pm r^2 \delta \tau \left( q_X^{\text{ch,A}} + q_X^{\text{ch,B}} \right) + \left( 2q^{\text{ch}} - \left( p_0 (q^{\text{con}} + q^{\text{div}}) + p \left( q_X^{\text{ch,A}} + q_X^{\text{ch,B}} \right) \right) \right) S_F \tag{58}$$

$$\frac{1}{\epsilon} \frac{dq_X^{\text{rec}}}{dt} = \pm r^2 \delta\tau q_0^{\text{rec}} + (q_X^{\text{rec}} - (1 - p_0)(q_X^{\text{rec}} + pp_0)) S_F \quad (59)$$

$$\frac{1}{\epsilon} \frac{dq_X^{\text{div}}}{dt} = \pm r^2 \delta\tau q_0^{\text{div}} + \left( q_X^{\text{div}} - (pq_0^{\text{div}} + p_0 q_X^{\text{ch,B}}) \right) S_F \quad (60)$$

$$\frac{1}{\epsilon} \frac{dq_X^{\text{con}}}{dt} = \pm r^2 \delta\tau q_0^{\text{con}} + \left( q_X^{\text{con}} - (pq_0^{\text{con}} + p_0 q_X^{\text{ch,A}}) \right) S_F \quad (61)$$

$$\frac{1}{\epsilon} \frac{dq_X^{\text{ch,A}}}{dt} = \pm r^2 \delta\tau q_0^{\text{ch}} + \left( q_X^{\text{ch,A}} - (pq_0^{\text{ch}} + p_0 q_X^{\text{con}}) \right) S_F \quad (62)$$

$$\frac{1}{\epsilon} \frac{dq_X^{\text{ch,B}}}{dt} = \pm r^2 \delta\tau q_0^{\text{ch}} + \left( q_X^{\text{ch,B}} - (pq_0^{\text{ch}} + p_0 q_X^{\text{div}}) \right) S_F \quad (63)$$

## Acknowledgments

## References

1. Bullmore E, Sporns O (2009) Complex brain networks: graph theoretical analysis of structural and functional systems. *Nature Reviews Neuroscience* 10: 186–198.
2. Markram H (1997) A network of tufted layer 5 pyramidal neurons. *Cerebral Cortex* 7: 523–533.
3. Perin R, Berger TK, Markram H (2011) A synaptic organizing principle for cortical neuronal groups. *Proceedings of the National Academy of Sciences* 108: 5419–5424.
4. Song S, Sjöström PJ, Reigl M, Nelson S, Chklovskii DB (2005) Highly nonrandom features of synaptic connectivity in local cortical circuits. *PLoS Biol* 3: e68.
5. Yoshimura Y, Dantzker JLM, Callaway EM (2005) Excitatory cortical neurons form fine-scale functional networks. *Nature* 433: 868–873.
6. Ko H, Hofer SB, Pichler B, Buchanan KA, Sjöström PJ, et al. (2011) Functional specificity of local synaptic connections in neocortical networks. *Nature* 473: 87–91.
7. Yassin L, Benedetti BL, Jouhanneau JS, Wen JA, Poulet JFA, et al. (2010) An embedded subnetwork of highly active neurons in the neocortex. *Neuron* 68: 1043–1050.
8. Zhao L, Beverlin BI, Netoff T, Nykamp DQ (2011) Synchronization from second order network connectivity statistics. *Frontiers in Computational Neuroscience* 5: 28.
9. Litwin-Kumar A, Doiron B (2012) Slow dynamics and high variability in balanced cortical networks with clustered connections. *Nature Neuroscience* 15: 1498–1505.
10. Gaiteri C, Rubin JE (2011) The interaction of intrinsic dynamics and network topology in determining network burst synchrony. *Frontiers in computational neuroscience* 5.
11. Kriener B, Tetzlaff T, Aertsen A, Diesmann M, Rotter S (2008) Correlations and population dynamics in cortical networks. *Neural computation* 20: 2185–2226.
12. Pernice V, Staude B, Cardanobile S, Rotter S (2011) How structure determines correlations in neuronal networks. *PLoS Comput Biol* 7: e1002059.
13. Trousdale J, Hu Y, Shea-Brown E, Josić K (2012) Impact of network structure and cellular response on spike time correlations. *PLoS Computational Biology* 8: e1002408.

14. Hu Y, Trousdale J, Josić K, Shea-Brown E (2013) Motif statistics and spike correlations in neuronal networks. *Journal of Statistical Mechanics: Theory and Experiment* 2013: P03012.
15. Bi Gq, Poo Mm (1998) Synaptic modifications in cultured hippocampal neurons: dependence on spike timing, synaptic strength, and postsynaptic cell type. *The Journal of Neuroscience* 18: 10464–10472.
16. Markram H (1997) Regulation of synaptic efficacy by coincidence of postsynaptic APs and EPSPs. *Science* 275: 213–215.
17. Abbott LF, Nelson SB (2000) Synaptic plasticity: taming the beast. *Nature neuroscience* 3: 1178–1183.
18. Caporale N, Dan Y (2008) Spike timing–dependent plasticity: A hebbian learning rule. *Annual Review of Neuroscience* 31: 25–46.
19. Markram H, Gerstner W, Sjöström PJ (2011) A history of spike-timing-dependent plasticity. *Frontiers in Synaptic Neuroscience* 3.
20. Song S, Miller KD, Abbott LF (2000) Competitive hebbian learning through spike-timing-dependent synaptic plasticity. *Nature Neuroscience* 3: 919–926.
21. Harris KD (2005) Neural signatures of cell assembly organization. *Nature Reviews Neuroscience* 6: 399–407.
22. Hebb DO (1949) *The organization of behavior: a neuropsychological theory*. Mahwah, N.J.: L. Erlbaum Associates.
23. Buzsáki G (2010) Neural syntax: cell assemblies, synapsembles, and readers. *Neuron* 68: 362–385.
24. Harris KD, Mrsic-Flogel TD (2013) Cortical connectivity and sensory coding. *Nature* 503: 51–58.
25. Kempster R, Gerstner W, Van Hemmen JL (2001) Intrinsic stabilization of output rates by spike-based hebbian learning. *Neural Computation* 13: 2709–2741.
26. Babadi B, Abbott LF (2010) Intrinsic stability of temporally shifted spike-timing dependent plasticity. *PLoS Comput Biol* 6: e1000961.
27. Guetig R, Aharonov R, Rotter S, Sompolinsky H (2003) Learning input correlations through nonlinear temporally asymmetric hebbian plasticity. *The Journal of neuroscience* 23: 3697–3714.
28. Rubin J, Lee D, Sompolinsky H (2001) Equilibrium properties of temporally asymmetric hebbian plasticity. *Physical Review Letters* 86: 364–367.
29. Kempster R, Gerstner W, Van Hemmen JL (1999) Hebbian learning and spiking neurons. *Physical Review E* 59: 4498.
30. Meffin H, Besson J, Burkitt AN, Grayden DB (2006) Learning the structure of correlated synaptic subgroups using stable and competitive spike-timing-dependent plasticity. *Physical Review E* 73: 041911.
31. Gilson M, Burkitt AN, Grayden DB, Thomas DA, Hemmen JL (2009) Emergence of network structure due to spike-timing-dependent plasticity in recurrent neuronal networks IV: Structuring synaptic pathways among recurrent connections. *Biological Cybernetics* 101: 427–444.

32. Fiete IR, Senn W, Wang CZH, Hahnloser RHR (2010) Spike-time-dependent plasticity and heterosynaptic competition organize networks to produce long scale-free sequences of neural activity. *Neuron* 65: 563–576.
33. Izhikevich EM, Gally JA, Edelman GM (2004) Spike-timing dynamics of neuronal groups. *Cerebral Cortex* 14: 933–944.
34. Morrison A, Aertsen A, Diesmann M (2007) Spike-timing-dependent plasticity in balanced random networks. *Neural Computation* 19: 1437–1467.
35. Babadi B, Abbott LF (2013) Pairwise analysis can account for network structures arising from spike-timing dependent plasticity. *PLoS Computational Biology* 9: e1002906.
36. Litwin-Kumar A, Doiron B (2014) Formation and maintenance of neuronal assemblies through synaptic plasticity. *Nature Communications* 5.
37. Karbowski J, Ermentrout G (2002) Synchrony arising from a balanced synaptic plasticity in a network of heterogeneous neural oscillators. *Physical Review E* 65.
38. Burkitt AN, Gilson M, Hemmen JL (2007) Spike-timing-dependent plasticity for neurons with recurrent connections. *Biological Cybernetics* 96: 533–546.
39. Gilson M, Burkitt AN, Grayden DB, Thomas DA, Hemmen JL (2009) Emergence of network structure due to spike-timing-dependent plasticity in recurrent neuronal networks III: Partially connected neurons driven by spontaneous activity. *Biological Cybernetics* 101: 411–426.
40. Gilson M, Burkitt AN, Grayden DB, Thomas DA, Hemmen JL (2009) Emergence of network structure due to spike-timing-dependent plasticity in recurrent neuronal networks. i. input selectivity–strengthening correlated input pathways. *Biological Cybernetics* 101: 81–102.
41. Gilson M, Burkitt AN, Grayden DB, Thomas DA, Hemmen JL (2010) Emergence of network structure due to spike-timing-dependent plasticity in recurrent neuronal networks v: self-organization schemes and weight dependence. *Biological Cybernetics* 103: 365–386.
42. Doiron B, Lindner B, Longtin A, Maler L, Bastian J (2004) Oscillatory activity in electrosensory neurons increases with the spatial correlation of the stochastic input stimulus. *Phys Rev Lett* 93.
43. Lindner B, Doiron B, Longtin A (2005) Theory of oscillatory firing induced by spatially correlated noise and delayed inhibitory feedback. *Phys Rev E* 72.
44. Gerstner W, Kempter R, van Hemmen JL, Wagner H (1996) A neuronal learning rule for sub-millisecond temporal coding. *Nature* 383: 76–78.
45. Fourcaud-Trocme N, Hansel D, van Vreeswijk C, Brunel N (2003) How spike generation mechanisms determine the neuronal response to fluctuating inputs. *Journal of Neuroscience* 23: 11628–11640.
46. Jolivet R, Lewis TJ, Gerstner W (2004) Generalized integrate-and-fire models of neuronal activity approximate spike trains of a detailed model to a high degree of accuracy. *Journal of Neurophysiology* 92: 959–976.
47. Jolivet R, Shurmann F, Berger TK, Naud R, Gerstner W, et al. (2008) The quantitative single-neuron modeling competition. *Biological Cybernetics* 99: 417–426.
48. Gardiner C (1985) *Stochastic methods*. Springer-Verlag, Berlin–Heidelberg–New York–Tokyo.



49. Gilson M, Burkitt AN, Grayden DB, Thomas DA, Hemmen JL (2009) Emergence of network structure due to spike-timing-dependent plasticity in recurrent neuronal networks. II. input selectivity—symmetry breaking. *Biological Cybernetics* 101: 103–114.
50. Feldman DE (2012) The spike-timing dependence of plasticity. *Neuron* 75: 556–571.
51. Froemke RC, Dan Y (2002) Spike-timing-dependent synaptic modification induced by natural spike trains. *Nature* 416: 433–438.
52. Kozloski J, Cecchi GA (2010) A theory of loop formation and elimination by spike timing-dependent plasticity. *Frontiers in Neural Circuits* 4.
53. Kunkel S, Diesmann M, Morrison A (2011) Limits to the development of feed-forward structures in large recurrent neuronal networks. *Frontiers in Computational Neuroscience* 4.
54. Galan R, Fourcaud-Trocme N, Ermentrout B, Urban NN (2006) Correlation-induced synchronization of oscillations in olfactory bulb neurons. *J Neurosci* 26: 3646–3655.
55. de la Rocha J, Doiron B, Shea-Brown E, Josić K, Reyes A (2007) Correlation between neural spike trains increases with firing rate. *Nature* 448: 802–6.
56. Shea-Brown E, Josić K, de la Rocha J, Doiron B (2008) Correlation and synchrony transfer in integrate-and-fire neurons: basic properties and consequences for coding. *Phys Rev Lett* 100.
57. Hong S, Ratte S, Prescott SA, De Schutter E (2012) Single neuron firing properties impact correlation-based population coding. *J Neurosci* 32: 1413–1428.
58. Ocker GK, Doiron B (2014) Kv7 channels regulate pairwise spiking covariability in health and disease. *Journal of Neurophysiology* 112: 340–352.
59. Deger M, Schwalger T, Naud R, Gerstner W (2013) Dynamics of interacting finite-sized networks of spiking neurons with adaptation. *arXiv:13114206 [q-bio]* .
60. Renart A, de la Rocha J, Bartho P, Hollender L, Parga N, et al. (2010) The asynchronous state in cortical circuits. *Science* 327: 587–590.
61. Brunel N (2000) Dynamics of sparsely connected networks of excitatory and inhibitory spiking neurons. *Journal of Computational Neuroscience* 8: 183–208.
62. Litwin-Kumar A, Chacron MJ, Doiron B (2012) The spatial structure of stimuli shapes the timescale of correlations in population spiking activity. *PLoS Comput Biol* .
63. Litwin-Kumar A, Oswald AMM, Urban NN, Doiron B (2011) Balanced synaptic input shapes the correlation between neural spike trains. *PLoS Comput Biol* 7: e1002305.
64. Levy N, Horn D, Meilijson I, Ruppin E (2001) Distributed synchrony in a cell assembly of spiking neurons. *Neural Networks: The Official Journal of the International Neural Network Society* 14: 815–824.
65. Mongillo G, Curti E, Romani S, Amit DJ (2005) Learning in realistic networks of spiking neurons and spike-driven plastic synapses. *The European Journal of Neuroscience* 21: 3143–3160.
66. Liu JK, Buonomano DV (2009) Embedding multiple trajectories in simulated recurrent neural networks in a self-organizing manner. *The Journal of Neuroscience: The Official Journal of the Society for Neuroscience* 29: 13172–13181.

67. Chen CC, Jasnaw D (2010) Mean-field theory of a plastic network of integrate-and-fire neurons. *Physical Review E* 81: 011907.
68. Mayer J, Ngo HVV, Schuster HG (2012) Dynamical mean-field equations for a neural network with spike timing dependent plasticity. *Journal of Statistical Physics* 148: 677–686.
69. Sjöström PJ, Turrigiano GG, Nelson SB (2001) Rate, timing, and cooperativity jointly determine cortical synaptic plasticity. *Neuron* 32: 1149–1164.
70. Bi GQ, Wang HX (2002) Temporal asymmetry in spike timing-dependent synaptic plasticity. *Physiology & Behavior* 77: 551–555.
71. Wang HX, Gerkin RC, Nauen DW, Bi GQ (2005) Coactivation and timing-dependent integration of synaptic potentiation and depression. *Nature Neuroscience* 8: 187–193.
72. Wittenberg GM, Wang SSH (2006) Malleability of spike-timing-dependent plasticity at the CA3–CA1 synapse. *The Journal of Neuroscience* 26: 6610–6617.
73. Pfister JP, Gerstner W (2006) Triplets of spikes in a model of spike timing-dependent plasticity. *The Journal of Neuroscience* 26: 9673–9682.
74. Clopath, Claudia, Büsing, Lars, Vasilaki, Eleni, Gerstner, Wulfram (2010) Connectivity reflects coding: a model of voltage-based STDP with homeostasis. *Nat Neurosci* 13: 344–352.
75. Shouval HZ, Bear MF, Cooper LN (2002) A unified model of NMDA receptor-dependent bidirectional synaptic plasticity. *Proceedings of the National Academy of Sciences of the United States of America* 99: 10831–10836.
76. Rubin JE, Gerkin, RC, Bi, G-Q, Chow, C (2005) Calcium time course as a signal for spike-timing-dependent plasticity. *Journal of Neurophysiology* 93: 2600–2613.
77. Graupner M, Brunel N (2012) Calcium-based plasticity model explains sensitivity of synaptic changes to spike pattern, rate, and dendritic location. *Proceedings of the National Academy of Sciences* 109: 3991–3996.
78. Churchland AK, Kiani R, Chaudhuri R, Wang XJ, Pouget A, et al. (2011) Variance as a signature of neural computations during decision making. *Neuron* 69: 818–831.
79. Kohn A, Smith MA (2005) Stimulus dependence of neuronal correlation in primary visual cortex of the macaque. *J Neurosci* 25: 3661–3673.
80. Churchland MM, Yu BM, Cunningham JP, Sugrue LP, Cohen MR, et al. (2010) Stimulus onset quenches neural variability: a widespread cortical phenomenon. *Nature Neuroscience* 13: 369–378.
81. Arieli A, Sterkin A, Grinvald A, Aertsen A (1996) Dynamics of ongoing activity: Explanation of the large variability in evoked cortical responses. *Science* 273: 1868–1871.
82. Tsodyks M, Kenet T, Grinvald A, Arieli A (1999) Linking spontaneous activity of single cortical neurons and the underlying functional architecture. *Science* 286: 1943–1946.
83. Royer S, Paré D (2003) Conservation of total synaptic weight through balanced synaptic depression and potentiation. *Nature* 422: 518–522.
84. Renart A, Song P, Wang XJ (2003) Robust spatial working memory through homeostatic synaptic scaling in heterogeneous cortical networks. *Neuron* 38: 473–485.

85. Lazar A, Pipa G, Triesch J (2009) SORN: a self-organizing recurrent neural network. *Frontiers in Computational Neuroscience* 3: 23.
86. Zheng P, Dimitrakakis C, Triesch J (2013) Network self-organization explains the statistics and dynamics of synaptic connection strengths in cortex. *PLoS Comput Biol* 9: e1002848.
87. Zenke F, Hennequin G, Gerstner W (2013) Synaptic plasticity in neural networks needs homeostasis with a fast rate detector. *PLoS Comput Biol* 9: e1003330.
88. Lefort S, Tómm C, Sarría JCF, Petersen CCH (2009) The excitatory neuronal network of the c2 barrel column in mouse primary somatosensory cortex. *Neuron* 61: 301–316.
89. Rubin JE (2001) Steady states in an iterative model for multiplicative spike-timing-dependent plasticity. *Network: Computation in Neural Systems* 12: 131–140.
90. Gilson M, Fukai T (2011) Stability versus neuronal specialization for STDP: Long-tail weight distributions solve the dilemma. *PLoS ONE* 6: e25339.
91. Richardson M (2007) Firing-rate response of linear and nonlinear integrate-and-fire neurons to modulated current-based and conductance-based synaptic drive. *Phys Rev E* 76: 021919.
92. Richardson M (2008) Spike-train spectra and network response functions for non-linear integrate-and-fire neurons. *Biol Cybern* 99: 381–392.
93. Cox D, Isham V (1980) *Point Processes*. Monographs on Statistics and Applied Probability. CRC Press.

## Tables

**Table 1. Model parameters**

Parameter	Description	Value
$C$	Membrane capacitance	$1 \mu\text{F}/\text{cm}^2$
$g_L$	Leak conductance	$0.1\text{mS}/\text{cm}^2$
$V_L$	Leak reversal potential	-72 mV
$\Delta$	Action potential steepness	1.4 mV
$V_T$	Action potential initiation threshold	-48 mV
$V_{th}$	Action potential threshold	30 mV
$V_{re}$	Action potential reset	-72 mV
$\tau_{ref}$	Action potential width	2 ms
$\mu$	External input mean	$1 \mu\text{A}/\text{cm}^2$
$\sigma$	External input standard deviation	9 mV
$N$	Number of neurons	1000
$p_0$	Connection density	.15
$W^{\max}$	Maximum synaptic weight	$5 \mu\text{A}/\text{cm}^2$
$\tau_S$	Synaptic time constant	5 ms

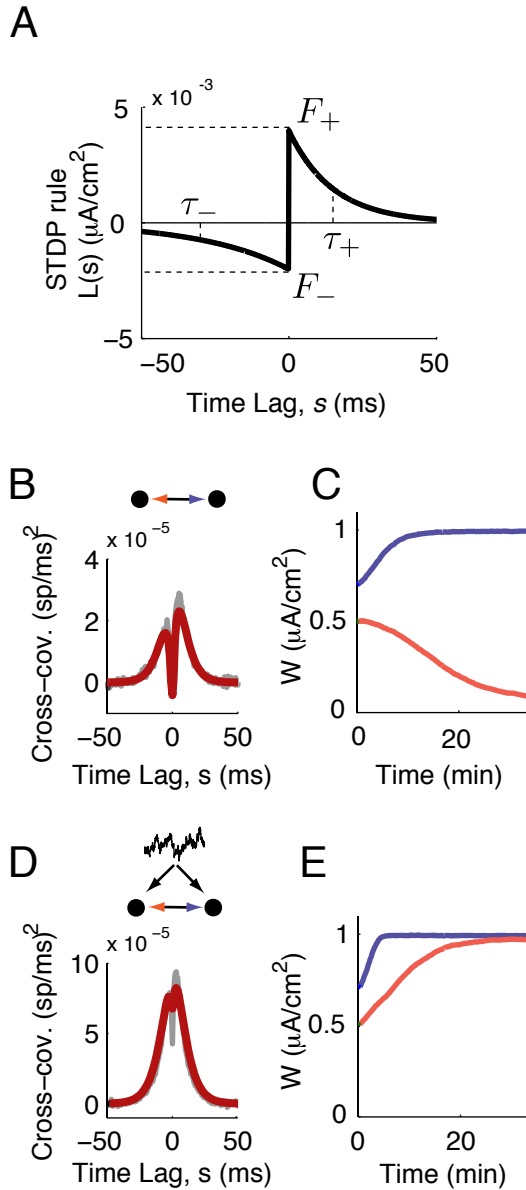


**Figure 1. Network structure shapes synaptic plasticity.** (A) The STDP rule,  $L(s)$ , is composed of exponential windows for depression (-) and potentiation (+). Each is defined by its amplitude  $f_{\pm}$  and timescale  $\tau_{\pm}$ . (B) Spike train cross-covariance function for a pair of neurons with no common input, so that synapses between the two neurons are the only source of spiking covariability. Shaded lines: simulation, solid lines: theory (Eq. (4)). (C,E) Synaptic weight (peak EPSC amplitude) as a function of time in the absence (C) and presence (E) of common input. (D) Spike train cross-covariance function for a pair of neurons with common input,  $c = .05$ . Common input was modeled as an Ornstein-Uhlenbeck process with timescale 5 ms.

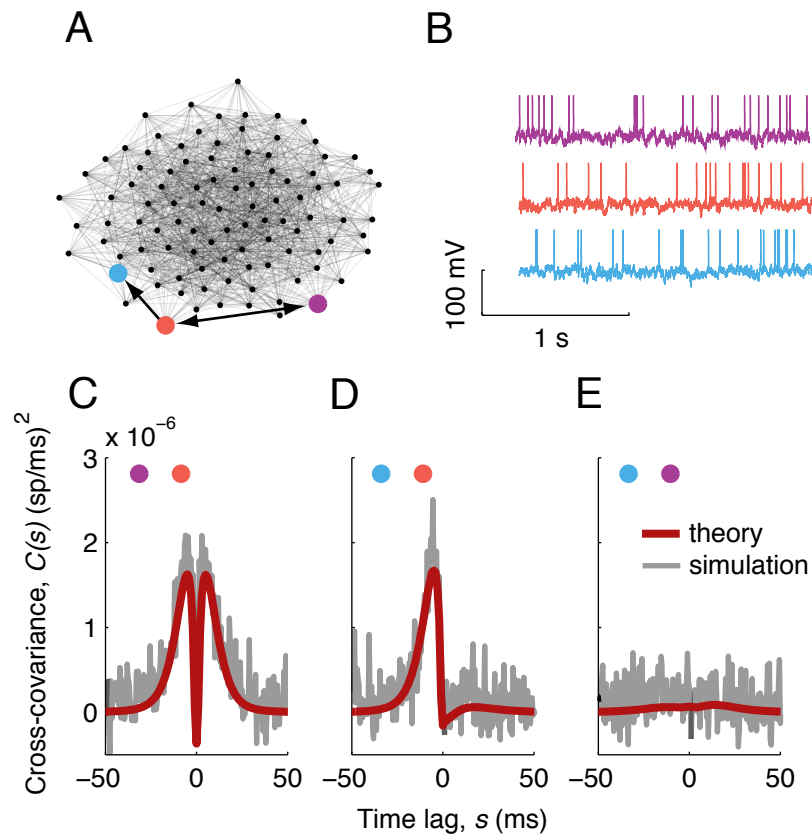


**Figure 2. Linear response theory for spike-train covariances.** (A) Illustration of the network connectivity for a subset of 100 neurons. Three neurons, and the connections between them, are highlighted. Nodes are positioned by the Fruchterman-Reingold force algorithm. (B) Example voltage traces for the three highlighted neurons. (C-E) Spike train cross-covariance functions for the three combinations of labeled neurons. Shaded lines: simulations, solid lines: linear response theory.

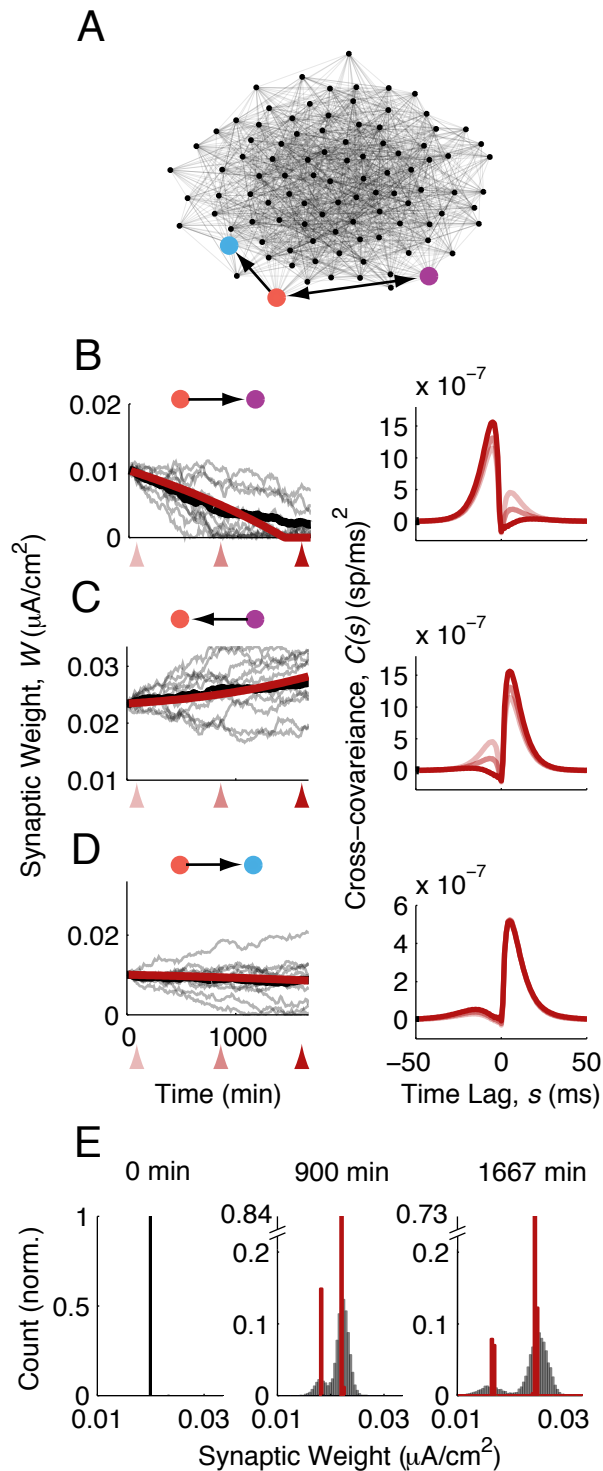


**Figure 3. STDP in recurrent networks with internally generated spiking covariability.** (A) As in Fig. 2A. (B-D) Left, Synaptic weight versus time for each of the three synapses in the highlighted network. Shaded lines: simulation, individual trials. Solid black lines: simulation, trial-average. Solid red lines: theory. Right, spike train cross-covariances at the three time points marked on the left (linear response theory). (E) Histogram of synaptic weights at three time points. Red, theory. Shaded: simulation.

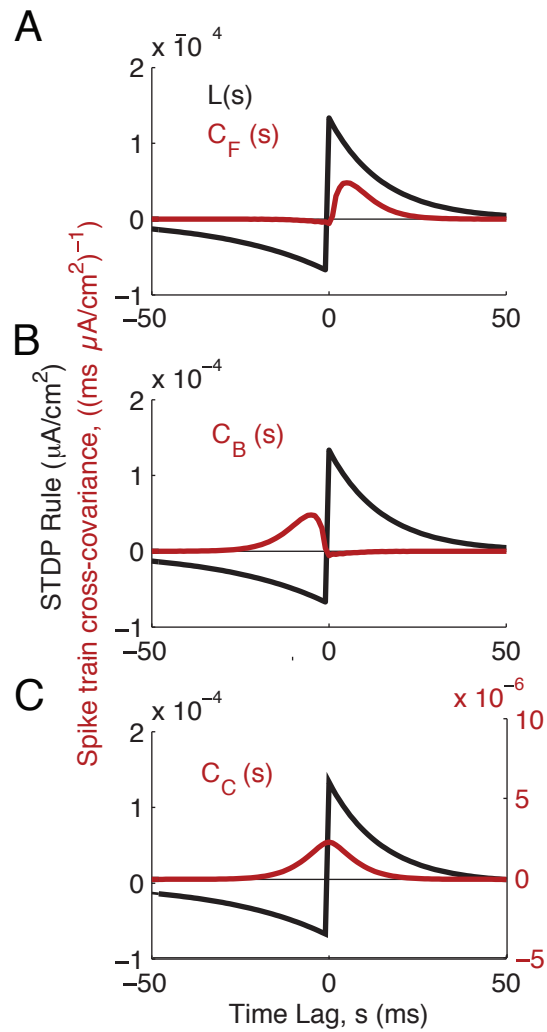


**Figure 4. Different sources of spike-train covariability interact with different parts of the STDP rule.** Black: STDP rule. Red: spike-train cross-covariances, from Eq. (7). (A) Covariance from forward connections interacts with the potentiation side of the STDP rule. (B) Covariance from backward connections interacts with the depression side of the STDP rule. (C) Covariance from common input is temporally symmetric and interacts with both the potentiation and depression sides of the STDP rule.



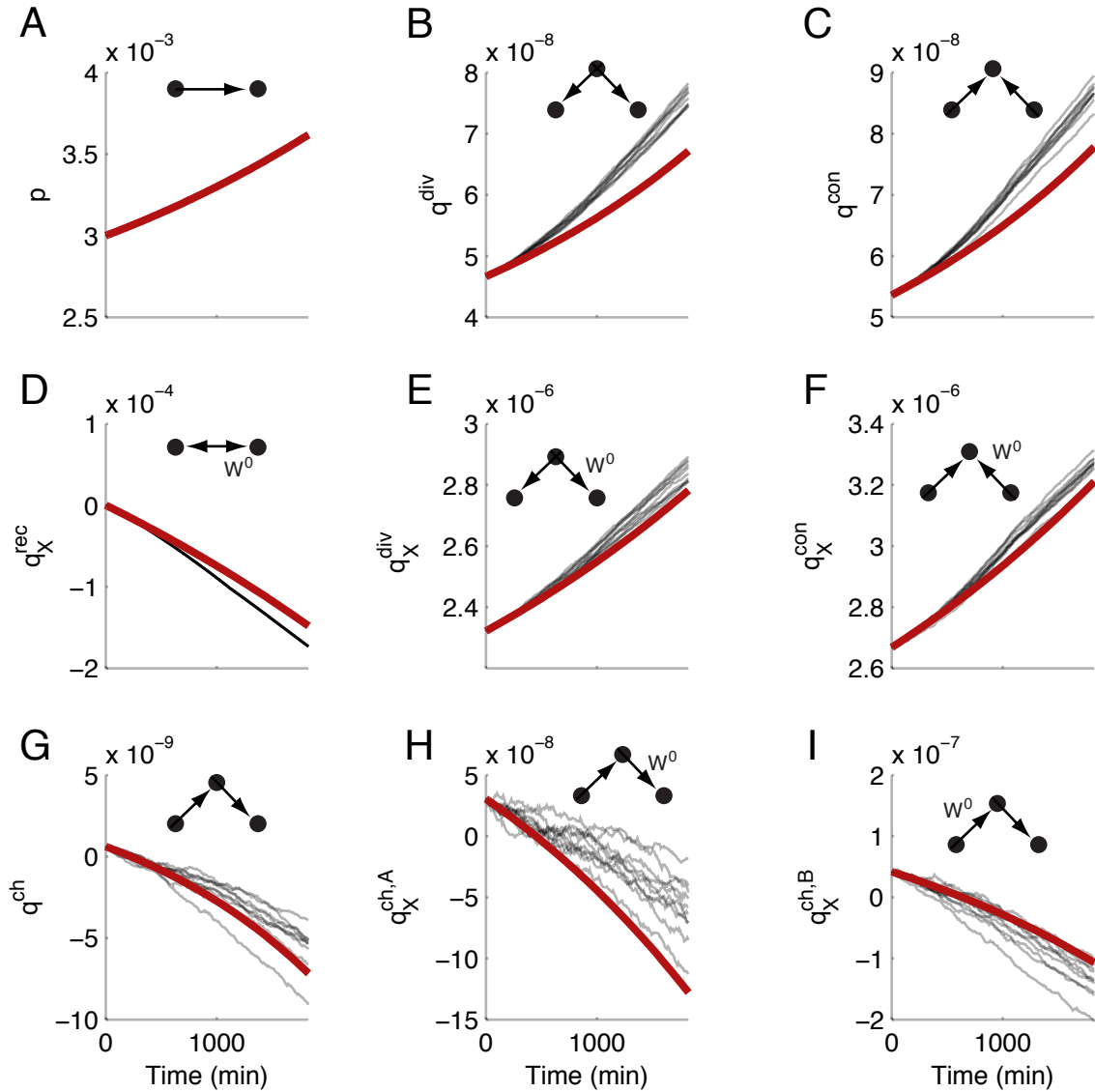


**Figure 5. Reduced theory for the plasticity of two-synapse motifs.** In each panel, the strength of a different motif or mixed motif is plotted as it evolves. (A) Mean connection strength. (B) Divergent motifs. (C) Convergent motifs. (D) Mixed recurrent motifs (strength of connections conditioned on their being part of a two-synapse loop). (E) Mixed divergent motifs (strength of individual synapses conditioned on their being part of a divergent motif). (F) Mixed convergent motifs. (G) Chain motifs. (H) Mixed chains type A (strength of individual synapses conditioned on their being the first in a chain). (I) Mixed chains type B (strength of individual synapses conditioned on their being the second in a chain). The STDP rule was in the depression-dominated balanced regime, as in Fig. 7B.

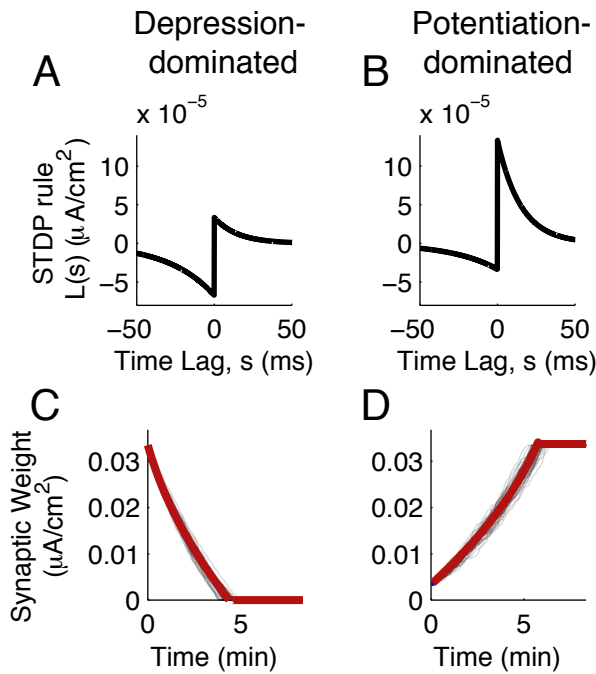


**Figure 6. Unbalanced plasticity gives rise to simple plasticity.** (A) A depression-dominated STDP rule: the amount of depression (integral of the depression side of the curve) is twice the amount of potentiation. (B) A potentiation-dominated STDP rule: the amount of potentiation is twice the amount of depression. (C) Evolution of synaptic weights with depression-dominated STDP: all weights depress. (D) Evolution of synaptic weights with potentiation-dominated STDP: all weights potentiate. Red lines: theory for mean synaptic weight. Shaded lines: simulation of individual synaptic weights.

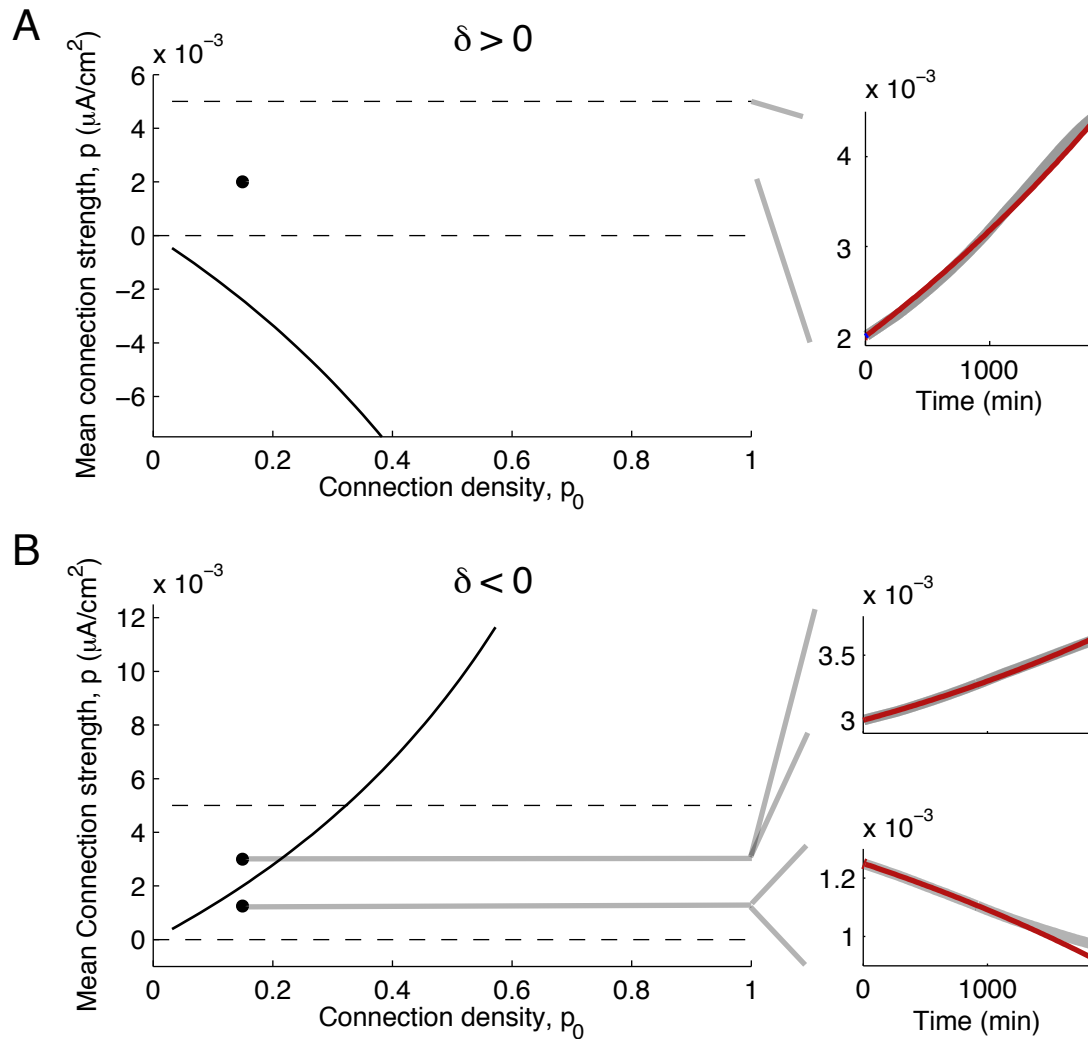


**Figure 7.** There is an invariant set in the motif space, corresponding to a network with independent synaptic weights. When the STDP is balanced between potentiation and depression, dynamics on this invariant set are quadratic in  $p$ , but only one of the two fixed points (the unstable one) is near the bounds  $[0, p_0 W^{\max}]$  (A) When the STDP rule is balanced and potentiation-dominated, the unstable fixed point is negative and decreases with the connection density so the mean connection strength always increases. (B) When the STDP rule is balanced and depression-dominated, the unstable fixed point is positive and increases with the connection density.

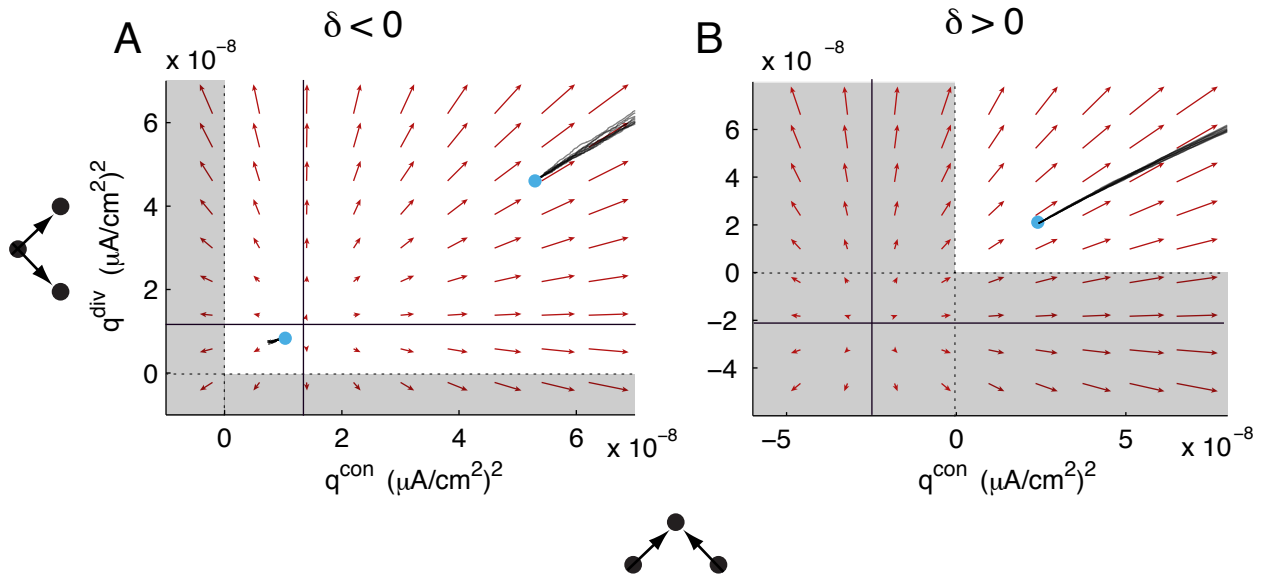


**Figure 8. Plasticity of convergent and divergent motifs with balanced STDP.** (A) Joint dynamics of convergent and divergent motifs when the STDP is balanced and depression-dominated. Initial conditions as in Fig. 7A. (B) Joint dynamics of convergent and divergent motifs when the STDP is balanced and potentiation-dominated. Initial conditions as in Fig. 7B. Red: the flow in the  $q^{\text{con}}, q^{\text{div}}$  slice of the motif phase space. Shaded black: plasticity of the motifs in simulations of the full spiking network. Cyan dots mark initial conditions for the simulations and each line is a realization. The vector fields are calculated with all other variables fixed at these initial conditions. For (A), the vector fields are similar for both sets of initial conditions.

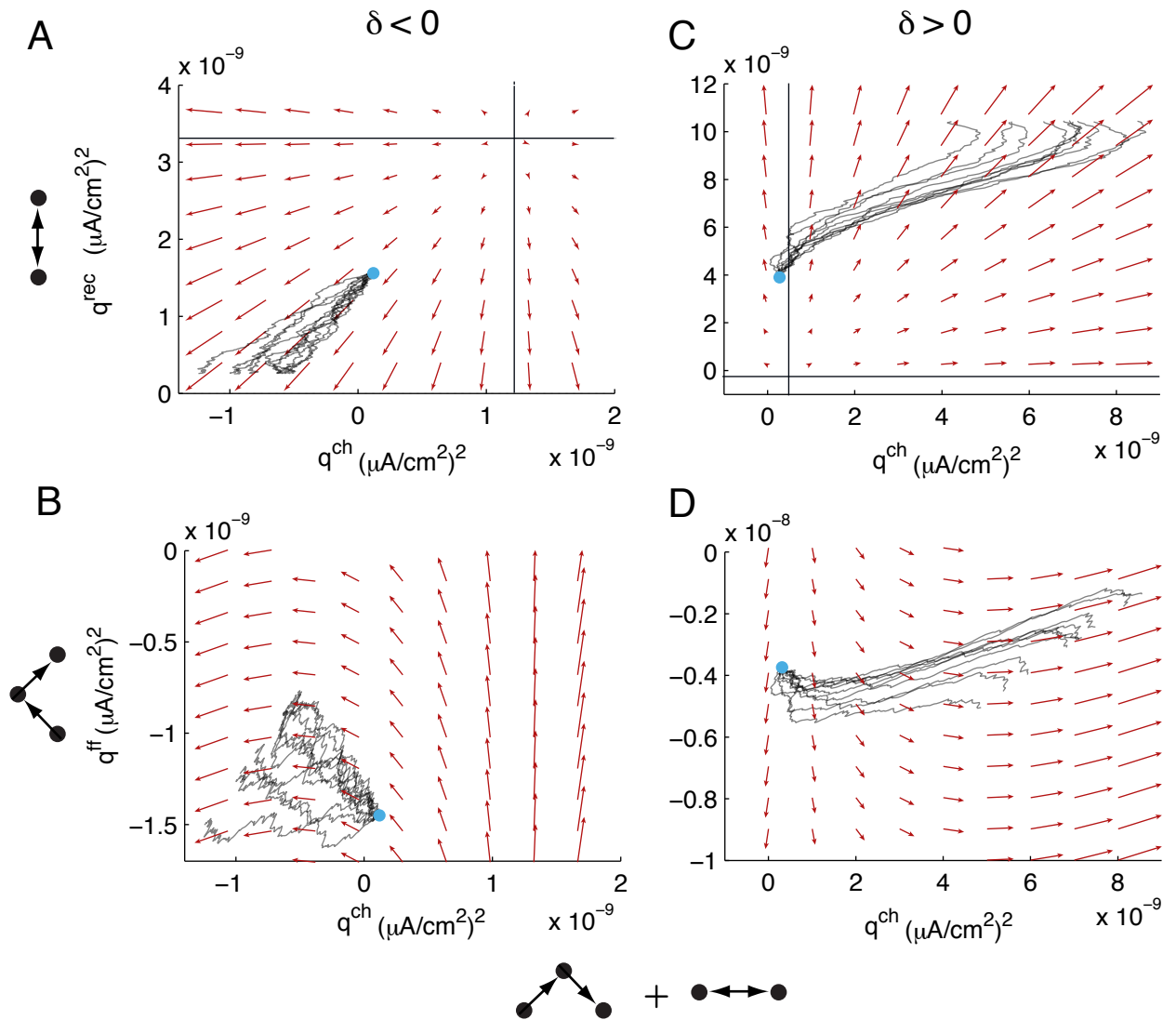


**Figure 9. Plasticity of loops and feedforward chains with balanced STDP.** (A,C) Joint dynamics of chains and feedforward motifs. (B,D) Joint dynamics of chains and recurrent motifs. Red: flow in the  $q^{\text{ch}}, q^{\text{rec}}$  or  $q^{\text{ch}}, q^{\text{ff}}$  slice of the motif space. Shaded black: plasticity of the motifs in simulations of the full spiking network. Cyan dots mark initial conditions for the simulations and each line is a realization. The vector fields are calculated with all other variables fixed at these initial conditions. Initial conditions for the depression-dominated balanced STDP rule (A,B) are as in Fig. 4 and Fig. 7B, top, and for the potentiation-dominated rule (C,D) as in Fig. 7A.